University of Kent

Canterbury

School of Physical Sciences

Investigation of Sterol uptake by a new Beta-Cyclodextrin Porous Network

August 2018

Student Name: Towseef Ishmum Ahmad

Student Number: 15909478

Programme: MSc by Research Chemistry

Project Advisor: Dr B. Blight and Dr J. Rossman

Abstract

This report details the synthesis and analysis of new β-cyclodextrin (β-CD) networks: ***KβCD-MOF-1***, ***KβCD-MOF-1-Chol*** and ***KβCD-MOF-2.*** Investigations of uptake of four sterols have also been conducted. The syntheses of the crystals were achieved by a vapour diffusion method at ambient temperature and pressure using mixtures of β-CD/potassium hydroxide in a ratio of 1:20, β-CD/potassium hydroxide/cholesterol in a ratio of 1:20:⅓ and β-CD/potassium benzoate in a ratio of 1:1, respectively. The analysis of crystals was performed using nuclear magnetic resonance (NMR) spectroscopy, X-ray diffraction (XRD) and optical and scanning electron microscopy. XRD showed KβCD-MOF-1 was made of accessible β-CD channels with each layer being perpendicular to the one above and the one below it. KβCD-MOF-1-Chol had a honeycomb like structure with cholesterol present in the β-CD channels. KβCD-MOF-2 was similar to a previously reported inclusion complex, although the crystallisation methods used were different.

Changes to crystal morphology of KβCD-MOF-1 and a control crystal were investigated using optical microscopy. The results of overnight soaking of these crystals using cholesterol dissolved in ethanol showed KβCD-MOF-1 crystal remained unchanged whilst the control crystal had nucleation occur on the edges.

Four types of sterols (Cholesterol, testosterone, beta-estradiol and deoxycholic acid) were used to investigate the uptake ratio of KβCD-MOF-1 and this was achieved using proton NMR analysis. The results showed that uptake of these sterols were successful. The NMR results also showed an inverse relation between numbers of polar groups in the sterol to the uptake by KβCD-MOF-1 network. The ratios of sterols:β-CD were observed to be 1:2, 1:4, 1:2 and 1:3 for cholesterol, testosterone, beta-estradiol and deoxycholic acid, respectively.

The encapsulations of UiO-66 crystals in to vesicles were investigated using fluorescence and electron microscopy. Although fluorescence microscopy provided some evidence of encapsulation however it was not confirmed by electron microscopy positively. Therefore the results remain inconclusive.

Acknowledgements

I would like to mark my heartfelt appreciation to Dr Barry Blight and Dr Jeremy Rossman for their constant support, feedback, constructive suggestion and supervision without which none of this work would have been possible.

I would also like to extend my gratitude to Dr Helena Shepherd for all her time and efforts in helping me to determine the crystal structures of many challenging samples. Thanks go to Yarry for helping with the powder diffractometer, as well as other MOF related queries, to Aga for her expertise with vesicles, to Dr Dan Mulvihill for capturing the detailed fluorescence crystal image and to Jed for his help with the TGA instrument. Many thanks to Barbora, Chrissie, Matt, Nafisa, Diego, Basma and also everyone in lab 310 and 134 for their constant encouragement, kind assistance and pleasant companies.

My stay in Kent has been made all the more pleasant by my friends and housemates and I would like to take the opportunity to thank them all.

Very special thanks goes to my beloved Mother Sayeda Ahmad and my father Dr. Ehsan Ahmad for their endless love and constant moral support during my stay away days in Kent and for coping with me when I was under pressure. A very special thanks for my younger brother Tahmid Ahmad for constantly bugging me with unscientific queries, without which my life in Kent would only be circulating around a scientific quest.

Finally, I thank the Almighty Allah for Allah's sustaining grace in my life and also for making it possible for me to complete my dissertation. To Allah alone be all the glory, praise and honour.

Table of Contents

1. Introduction

1.1 Metal Organic Frameworks

In the recent years, Metal organic frameworks (MOFs) have attracted considerable attention because they combine very high levels of porosity with a range of other functional properties that occur through the metal moiety and/or the organic ligands. These porous networks bear the potential of revolutionising applications such as gas storage and separation, drug delivery, carbon capture, bio-mimetic mineralisation or catalysis.[1-18]

The main constituents of MOFs are metal ions or clusters of metal ions and organic ligands or linkers. In order to synthesise MOFs a ligand forms more than one coordinate bond (multi-dentate ligands) which allows ligand to bond to several metal ions or metal ion clusters. Examples of metal ions or metal ion clusters used for MOFs are Zn_4O in MOF-5 and $Zr_6O_4(OH)_4$ cluster in UiO-66.[19] Figure 1-1 shows an example of a zinc-based MOF named MOF-5.

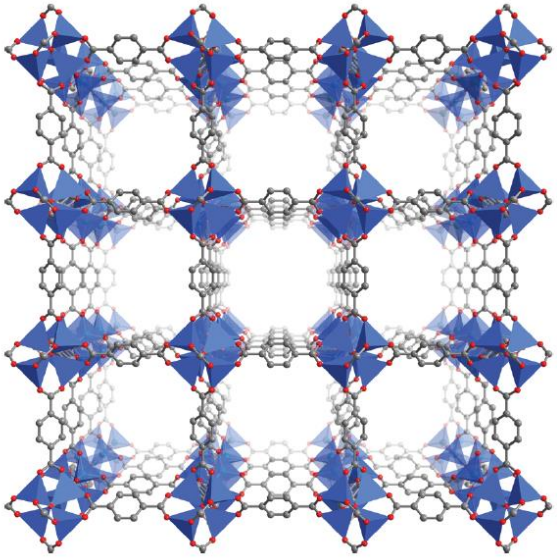

Figure1-1: An example of zinc-based MOF known as MOF-5. It is formed from Zn_4O nodes with 1,4-benzodicarboxylic acid/terephthalic acid ligands between the nodes.[6,7]

Examples of ligands (Figure 1-2) include molecules such as terephthalic acid which is used to make MOF-5.[20] Larger structures such as 2,3,6,7,10,11-hexaaminotriphenylene (HATP) have also been used to make MOFs which have high conductivity.[20] A mixture of ligands can be used to limit or control the structure of MOFs as smaller ligands can also be used to 'cap' a metal centre so that a certain size of structure can be obtained.[20,21]

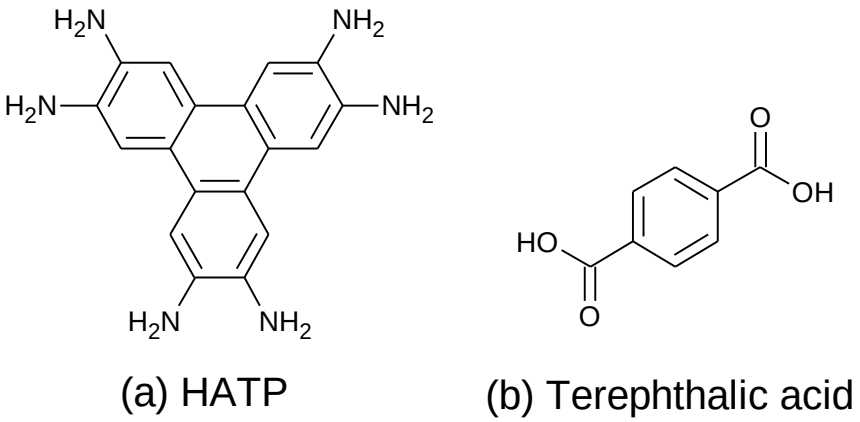

(a) HATP (b) Terephthalic acid

Figure 1-2: Structures of two ligands (a) HATP and (b) terephthalic acid.

The differences in shape and size of the ligands and the abundance of the metal ions or clusters mean that the combinations of MOFs which can be formed are almost limitless. The MOFs are crystalline therefore the exact location of the atoms and how they are connected are known. Hence, it is possible to synthesis materials with specific changes in chemical functionalities and matrices.

In this way, MOFs have been synthesised for a wide range of applications. These materials are utilised in the areas of gas separation, adsorption, catalysis and drug delivery,[21] examples include MOF-5, ZIF-8 and ZIF-9.[8] MOFs have been made using zinc and sodium for gas adsorption[9] and electrochemical applications.[15] Copper based MOFs have been reported as magnetic MOFs.[10] Zinc based MOFs such as MOF-5 and MOF-74 have been studied for post-synthesis modifications.[11] MOFs such as MIL-101 have been used as catalysts.[12]

Manganese based MOFs have been made for hydrogen adsorption.[13,17] IR-MOF-3 have been used as catalysts.[14] PPF-1 is another zinc based MOF.[16] UIO-68 has been used for hydrogen storage.[18]

The above list summarises some interesting applications of MOFs and these applications are among the few which inspired the synthesis of a new MOF that could be used for potential applications such as drug delivery. In the following section some further details of different applications of MOFs are given.

1.1.1 Applications of MOFs

Heterogeneous catalysts such as zeolites, porous solids and metal organic frameworks have shown potential as solid catalysts.[27] MOFs, in comparison to other crystalline structures, can be made with a large variety of metal nodes and organic linkers which arises to many different combinations that can be predicted and also can be interchanged during post-formation. As the solid catalysts MOFs offer additional points of coordination on the metal nodes, and as the linkers can be exchanged therefore additional site availability as well as change in porosity could be obtained. This in turn favours the use of MOFs alongside established inorganic porous materials.[27]

Several commercially available MOFs were used to demonstrate the potential of using premade MOFs in a variety of acid catalysed or aerobic oxidation reactions. The MOFs used in such applications included Fe(BTC), $Cu_3(BTC)_2$, Al(OH)(BDC) and $Zn(MeIm)_2$.[27]

Oxidation reactions utilise transition metal compounds as catalysts. The use of MOFs in such reactions could minimise the use of toxic transition metals as well as reduce the formations of hazardous or toxic waste materials.[27] In the studies conducted by Dhakshinamoorthy *et al.* of the four commercial MOFs

Fe(BTC) showed the highest catalytic activity. Current heterogeneous catalysts use metals such as Pd, Pt and Au. Using MOFs in the place of heavy metals as catalysts will reduce costs and also increase the selectivity of reactions. The key points for MOFs awaiting commercialisation are to increase the chemical and thermal stabilities such that the productivity of the catalysts can be used in industrial processes. Every year more MOF structures are being discovered and utilised to assist in various reactions, which previously relied on transition metal materials as the main catalyst.[27]

Porous hybrid inorganic-organic solids/metal organic frameworks show potential applications in fields of gas storage, adsorption, separation and catalysis are mainly microporous. The smaller size of these micro pores restricts the type of materials/drugs that could be used in the field of drug delivery. To overcome this shortfall and to produce MOFs with pores of sufficient size for drug delivery of different types, Horcajada *et al.* made chromium-based hybrid solids (MIL-100 and MIL-101) using a variety of carboxylic acids. These were used to demonstrate that pharmaceutical compounds could be delivered by highly porous network crystals. Ibuprofen was adsorbed into the crystals from a solution in hexane and the adsorption was determined with techniques such as elemental analysis and x-ray fluorescence. Both structures (MIL-100 and MIL-101) showed high adsorption of ibuprofen, with different linkers the crystals had varying adsorption values due to varying pore sizes.[28]

The burning of fossil fuels and the resulting atmospheric pollution including the release of carbon dioxide into the atmosphere is not desirable. Research into MOFs has shown that gas separation and adsorption of gases such as carbon dioxide and methane are possible. With the availability to fine tune MOFs, such as pore sizes, these materials could be used in tandem with membrane separation

techniques. The group of Neves had designed and characterised mixed matrix membranes (MMMs) which were made by incorporating porous MOFs into organic polymer structures.[29]

Established MOFs such as MOF-5 and MIL-101 were dispersed into an organic solution of Matrimid in various concentrations and then spread as a thin film to dry and form the MMMs. The mechanical properties (tension and elongation at break) decreased when the concentration of MOF was increased. Although the membrane became more rigid with the addition of MOF structures the permeation of gases increased. The structures of MOFs can be adapted for the selectivity of gases such as carbon dioxide, nitrogen or methane. This has shown that there is potential to use MOFs as a part of mixed matrix membranes to separate gaseous mixtures.[29]

Figure 1-3 shows a selection of MOFs which have been used for gas storage. The differences in ligands show that a wide variety of structures can be made either by changing the shape of a ligand by adding functional groups onto the structure or by using larger ligands with an extended network.[30]

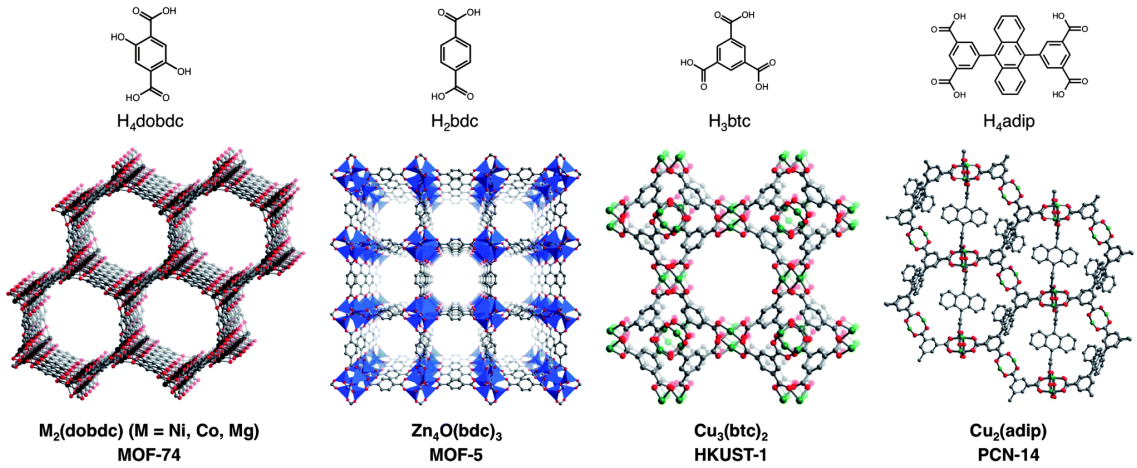

Figure 1-3: Examples of MOFs used for gas storage, ranging in shapes and sizes dependent on the ligands used.[30]

More and more new MOFs with a variety of functionalities have been discovered, and researchers are keen to determine effective applications for these materials.

As advances in the field have been made, chemists have strived to produce frameworks which do not generate hazardous bi-products as part of the overall synthesis.[25] Every potential new use of MOFs brings the challenge of determining a method of using more environmentally friendly materials which may yield the same outcome as using bulk stock such as hydrocarbons from crude oil. One way this was approached was by using starting chemicals derived from naturally occurring materials.[26]

The limitless possibility of combinations and applications for MOFs makes this area very fruitful for research.

1.2 Cyclodextrin

Cyclodextrins are cyclic compounds which are made of α-D-glucopyranose (glucose) units. It was discovered by the chemist Antoine Villiers in the late 19th century.[24] The glucopyranose units are joined together at carbons C1 and C4, this is known as α(1-4)-glycosidic bond, shown in figure 1-4. These types of bonds form when two or more sugar molecules join with one another by a loss of a water molecule at the positions one and four. When multiple sugars are joined together these classes of molecules are known as oligosaccharides. The most common structures are made of 6, 7 & 8 units, known as alpha (α), beta (β) and gamma (γ)-cyclodextrin respectively shown in figure 1-4.

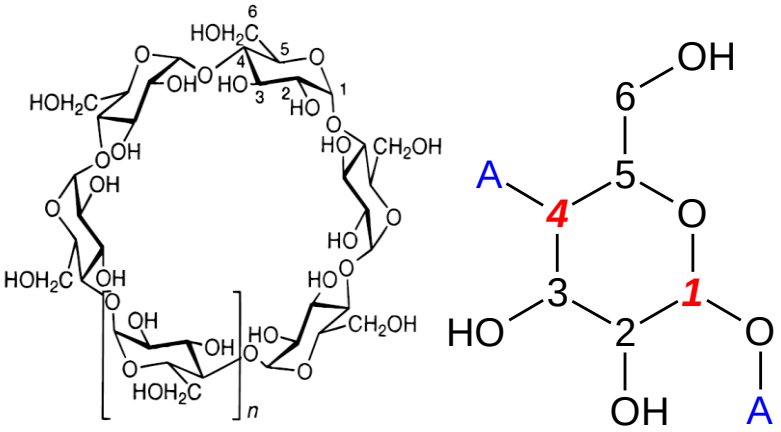

Figure 1-4: General structure of the most abundant cyclodextrins where n = 1, 2 and 3 are α-, β- and γ-cyclodextrin respectively (Left). Glucopyrnose unit with carbons highlighted to show the α(1-4)-glycosidic bond (Right).[24]

The structures of cyclodextrins are cone shaped with two faces. The primary face has the hydroxide group bonded to the methyl group (carbon 6) or primary carbons. The secondary face has the hydroxide groups bound directly to the central ring (carbon 2 and 3), or secondary carbons. When in solution the hydroxide groups are arranged such that all the groups point away from the central cavity of the cyclodextrin, this forms a hydrophobic environment in the central cavity (Figure 1-5).[31]

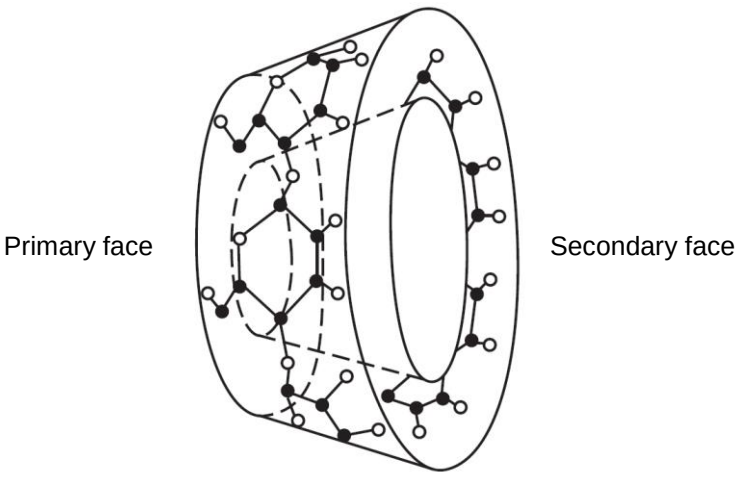

Figure 1-5: Structure of cyclodextrin showing the 3D orientation of the molecule.[31]

The outer hydroxide groups of cyclodextrin are more easily attracted to polar molecules whilst the inner cavity is then able to bind non-polar molecules such as hydrocarbons. This ability to bind non-polar compounds when in polar solutions has peaked research interest in this class of molecules.

The primary focus on CDs has been on α-CD and γ-CD due to the structures being symmetrical. Functionalised β-CD has seen uses in various industries as the additional groups opened more applications which improved upon different areas. Some notable examples of the use of functionalised β-CD over unaltered β-CD are methyl-β-CD and hydroxypropyl-β-CD.

Methyl-β-CD has been widely used in biology as an extractor of cholesterol from cell membranes, specifically because it forms a strong inclusion complex with cholesterol in solution.[23] Hydroxypropyl-β-CD has been used in the food industry throughout the world and is considered safe to use.[32] Figure 1-6 shows the positions at which CDs are substituted to form functionalised derivatives. In the case of methyl-CD the R groups are either hydrogen (H-) or CH_3 group and for hydroxypropyl-CD the R groups are either H- or $CH_2CHOHCH_3$ group.

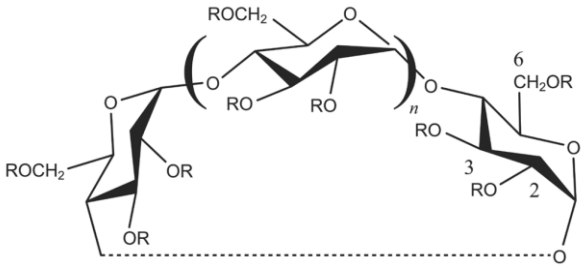

Figure 1-6: Structure of cyclodextrin showing the positions of substitution (R groups).[32]

1.2.1 CD-MOFs and applications

Recently a study was reported where γ-CD was used to make a new MOF which was biodegradable.[25,26] This was done by using food-grade materials (γ-CD and

KOH) in a vapour diffusion experiment. Vapour diffusion was achieved by mixing a ratio of 1:8 mmol of γ-CD and KOH in water then allowing slow diffusion of Everclear grain spirit (ethanol) over a few days.

The resulting structure was a highly porous, extended body-centred cubic crystalline material named CD-MOF-1. The primary face of γ-CD formed the inner face whilst the secondary face made up the outward face of the cube (Figure 1-7). The crystal structure revealed that each of the potassium (K) ions was coordinated to four γ-CD rings through four different glucopyranose units. Two of the glucopyranose units were coordinated through the secondary hydroxide groups whilst the other two units were coordinated through the glycosidic ring oxygen and the primary hydroxide group.

Another metal salt, rubidium hydroxide, was also used in a ratio of 1:8 with γ-CD as above.[25,26] The structure formed was also an extended body-centred cubic network and named CD-MOF-2. These γ-CD crystals share the same crystal structure but are different due to the use of different metals which link the CD units together. Figure 1-7 shows the cubic structure of CD-MOF-1 and CD-MOF-2.

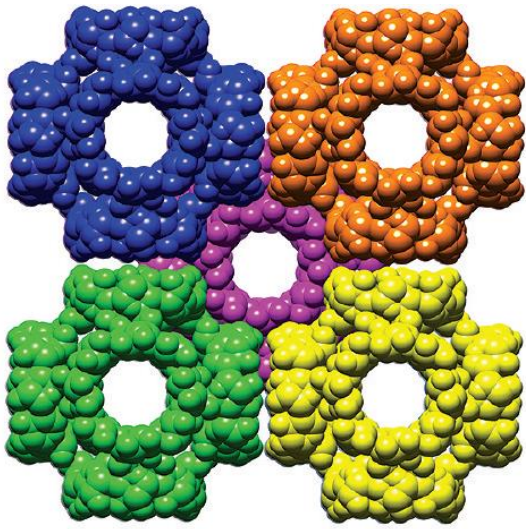

Figure 1-7: Structure shared by CD-MOF-1/CD-MOF-2 shown as a space filling representation of the body-centred cubic network.[25,26]

For modern drug delivery technologies increasing or enhancing the solubility and bioavailability of active pharmaceutical ingredients (APIs) has been desirable because a large number of potential compounds are hydrophobic. The central ring of CD forms hydrophobic cavities, as mentioned earlier. As CDs can form inclusion complexes which can shield hydrophobic structures in hydrophilic media, this feature makes CDs a good candidate as a material which can be used to enhance water solubility of hydrophobic APIs.[33]

Ibuprofen is used to treat inflammation in cells and also for possible cancers. This had already been entrapped in other MOFs such as UiO-66, however due to the toxic nature of the metals/linkers present in the structures it was not possible to carry out tests in vivo (in living tissue). CDs are considered to be safe to use (in edible products) and γ-CD can be hydrolysed by salivary α-amylase,[33] CD-MOFs could be used as part of new potential rapid drug delivery by oral ingestion.[33]

Two methods were used to study the uptake of ibuprofen: co-crystallisation and absorption. In both methods a racemic mixture of the (S)-(+) enantiomer (pharmaceutically active) and (R)-(-) enantiomer (pharmaceutically inactive and non-toxic) of ibuprofen was used. Further tests showed that CD-MOF-1 was not selective towards either enantiomer and uptakes of both were seen. An advantage of ibuprofen is that the non-toxic (R)-(-) enantiomer can be metabolised to form the other active enantiomer by a unidirectional chiral inversion.[33]

CD-MOF-1 has the potential to be utilised as an effective oral drug delivery media for pharmaceutical ingredients which are hydrophobic in nature. With ibuprofen it was shown that CD-MOF-1 could be prepared using potassium derivatives or even soaked in free acid forms and both methods showed positive results towards a rapid uptake/delivery mechanism.[33]

The porous structure CD-MOF-2 was found to be highly selective for the adsorption of carbon dioxide (CO_2) at low pressures.[34] The method by which CO_2 is captured in CD-MOF-2 is by reaction of the CO_2 molecules with free hydroxide groups to form carbonic acid. The process was found to be reversible. Favourable reactivity arises in CD-MOF-2 as γ-CD had many accessible hydroxyl groups at the circumference of the large pores (1.7 nm diameter). If the binding of carbon dioxide occurred by the formation of a carbonate ester (reaction of an OH group on CD with a CO_2 molecule), then it could be possible to view gaseous uptake by diffusing a readily available pH indicator.

The compound methyl red was diffused into the CD-MOF-2 network and when dried, formed yellow crystals due to deprotonation (anion metathesis). When exposed to any source of carbon dioxide the crystals changed colour to orange/red which showed a positive result for carbon dioxide. The crystals were cycled several times and did not show apparent fatigue. The uptake was only observed when the network was in a solid-crystalline state, as when the crystals were crushed no colour change was observed in the presence of carbon dioxide.
The ability for the crystal to capture carbon dioxide and that it can also be re-used multiple times (along with small coloured indicators) revealed that environmentally benign materials could be effectively used as a source of carbon fixation.[34]

The biocompatibility of materials is essential for applications of MOFs in biological systems. Metals such as Ca, Fe, Zn, Ti and K are considered as biologically acceptable [35] established by their oral lethal dose LD_{50} which is a single dose of a substance that causes the death of 50% of an animal population from exposure to that substance by any route other than inhalation. Therefore, interest has been growing to use biomolecules as linkers suitable to link together those metals in biologically active MOFs. Naturally occurring materials such as peptides,

carbohydrates, amino acids and a variety of compounds have been reported as being suitable to link together metal ions to form functional porous frameworks. One such example is the synthesis of environmentally friendly and renewable CD-MOFs obtained from γ-CD and K cations using -OCCO- linker which were used in drug absorption applications.[35]

Very few studies have focused on the hydrothermal, chemical and thermal stabilities of MOFs and CDMOFs when molecules such as various drugs are adsorbed into the framework.[35]

CD-MOFs are potential candidates in drug absorption applications. Liu *et al.* (2016) investigated absorption behaviour of 21 different drugs to γ-CD-MOF. Synthesis of CD-MOF was carried out by changing variables such as reactant concentrations and time and the crystalline stability was studied for different temperatures, solvents and humidity. It was demonstrated that drugs which had carboxyl groups present in them showed higher adsorption whereas drugs with nitrogen and other heterocyclic rings showed low adsorption.[35]

The unaltered form of β-CD has seen very little use in chemistry in contrast to functionalised β-CD because of weaker binding of molecules. Therefore this project will aim to show that unaltered β-CD can be used to effectively to form coordinate networks which will be able to replicate or come close to being similar to networks which are made of other similar ligands.

1.3 Vesicles

MOFs have been established as effective materials for drug delivery, such as chromium MOFs[28] and CD-MOFs[33] were used to bind ibuprofen.[33] Vesicles are also widely used in drug delivery[36] with the advantage that they can protect the inner contents from external environments. This feature has widely been utilised in drug delivery for treating cancers.

Vesicles are phospholipid bilayer capsules which can resemble the membranes of cells. Cell membranes are made of three main components: lipids including phospholipids and cholesterol, proteins, and carbohydrates as described in the fluid mosaic model of cell membranes.[37,38]

Phospholipids are a main part of cell membranes as the structure contains a phosphate group as a 'head' and this is connected to two fatty acid hydrocarbon tails. A bilayer is formed when two rows of phospholipids arrange so that the phosphate heads point outwards towards solvent, such as water, and the fatty acid hydrocarbons forms a middle layer (Figure 1-8, the idea was taken from the 3D model by Nicolson, 2014).[38]

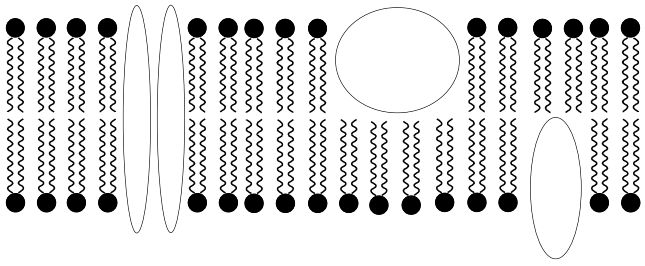

Figure 1-8: 2D schematic representation of phospholipid bi-layer where the phosphate groups (dark circles) point towards outer and inner solvent and the lipid tails form the inner (nonpolar) section of a cell membrane. Proteins are distributed throughout the membrane shown here as elliptical shapes.

Cholesterol is a crucial part of animal cells as this molecule helps to keep the cell membrane in a fluid state. The presence of cholesterol reduced the disorder in the lipid tails; this in turn caused the lipid tails to arrange equally throughout the bilayer membrane as shown in figure 1-9.[39]

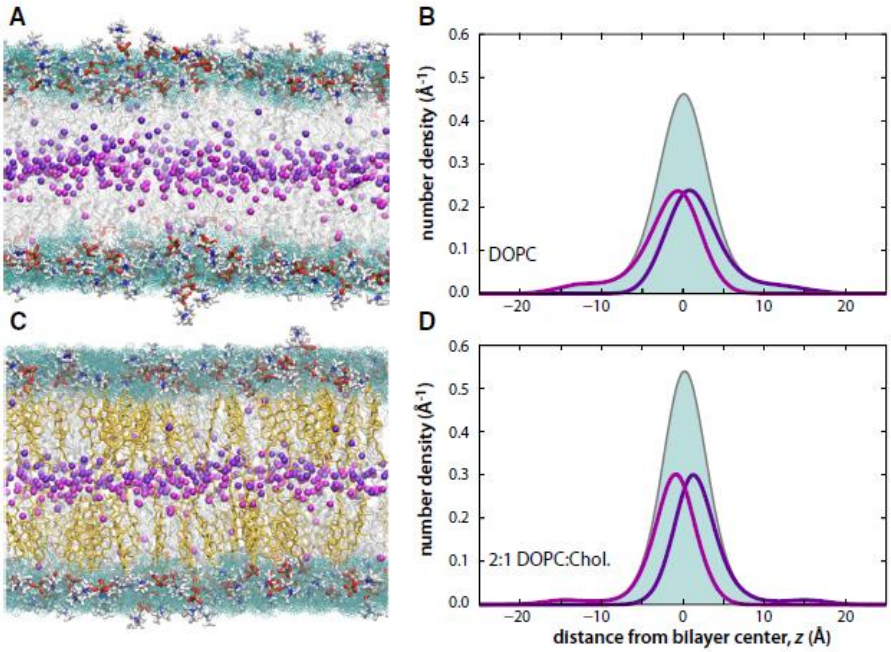

Figure 1-9: Molecular dynamics simulation of (A) DOPC only bilayer and (C) 2:1 ratio DOPC/cholesterol bilayer with terminal methyl groups as purple and magenta, acyl chains as grey and cholesterol shown as gold. (B) and (D) show the distribution of terminal methyl groups in respective bilayers.[39]

It was also observed that cholesterol in the presence of high-melting lipids (gel phase) and low-melting lipids (liquid-disordered l_d phase) causes a fluidising effect to the former and a condensing effect to the latter. This in turn brings the different lipids to an intermediate stage (liquid-ordered l_o phase) where the thickness, compactness and fluidity are neither too high or too low (Figure 1-10).[40]

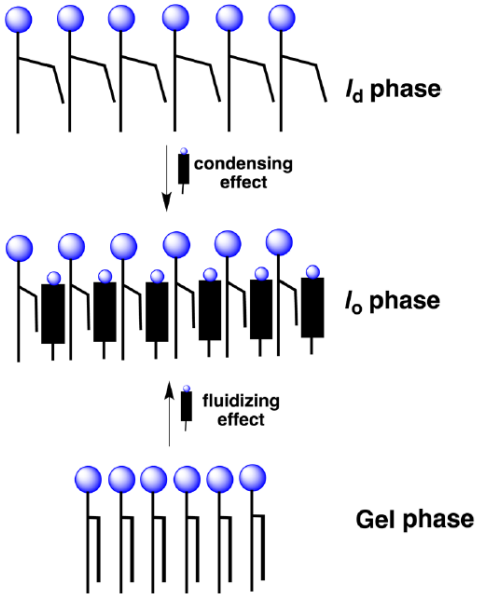

Figure 1-10: A general representation of the effects of cholesterol of low and high melting lipids.[40]

Unilamellar (single bilayer) vesicles are typically categorised into three main types by diameter, small <50 nm (SUVs), large <100 nm (LUVs) and giant >100 nm (GUVs). These have been used in a wide variety of applications such as studies of membrane protein interactions and lipid domain characteristics.[41] GUVs have been primarily used as cell mimicking models as the size of around 10µm, membrane curvature and phospholipid content can be made to be almost similar to animal cells.[42] The similarities to animal cells have led to a wide variety of studies in which GUVs have been used to simulate models of membrane interactions as well as effects of content and shape of vesicles in the presence of certain drugs or specific proteins.

Figure 1-11 shows various vesicles made from membrane lipid extracts as well as mixtures of lipids with and without cholesterol. The scale bars represent 10 µm. A fluorescence tagged molecule is typically incorporated into lipid mixtures to view them after formation process.

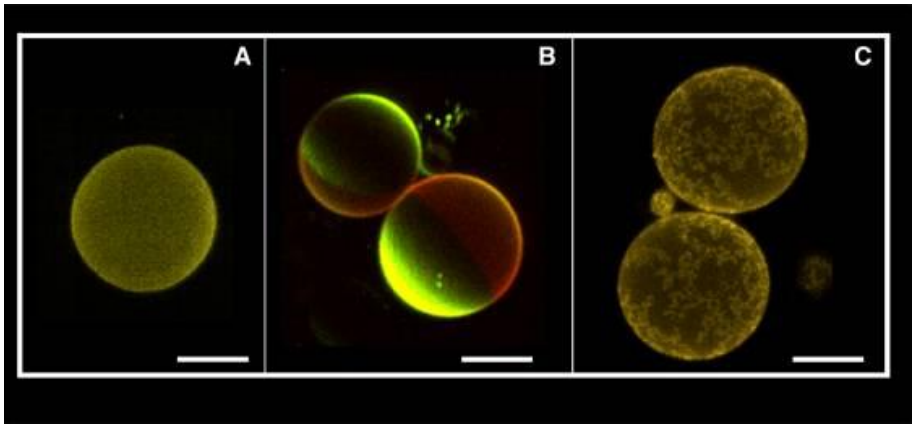

Figure 1-11: Fluorescence images of vesicles made using electroformation A) Vesicles made using red blood cell membrane lipid extracts B) Vesicles made from lipids and 20 mol% cholesterol and C) Vesicles made from lipids only without cholesterol. The scale bars shown represents 10 µm.[43]

A fluorescent derivative known as topfluor cholesterol (cholesterol with the hydrocarbon chain replaced by BODIPY group)[44] is also used to view vesicles (under blue light excitation). These help to distinguish a vesicle from surrounding medium. The bodipy group is a fluorophore component of the molecule which is hydrophobic and insensitive to changes in conditions such as polarity and pH. The structures of cholesterol and topfluor cholesterol are shown in Figure 1-12.

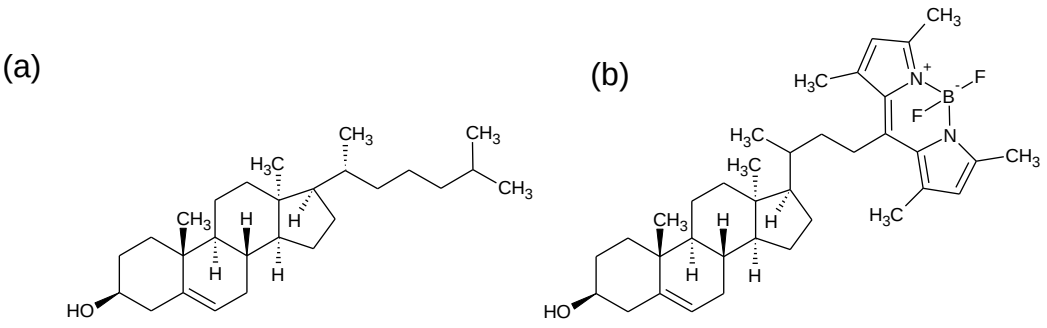

Figure 1-12: Structures of (a) cholesterol and (b)topfluor cholesterol, respectively.

There are many different methods to synthesise vesicles, dependent on the required size. The most typical methods are electroformation and extrusion.

The method of extrusion involves compressing a mixture of suspended lipids in a buffer solution through a series of fine filters and polycarbonate membranes using a pair of gas-tight syringes and a mini-extruder device. This is a long process and yields vesicles which have high sample reproducibility. Overall extrusion is a relatively slow process and requires manual handling of components.[45]

Electroformation involves applying an alternating current through a lipid solution suspended in an ionic buffer solution. There are various ways to perform this process. Indium Tin Oxide (ITO) coated slides with spacers have been used to form wells in which suspensions can be held and electrodes have been used directly placed in solutions as a surface for vesicle formation. This is a relatively fast process and yields vesicles with varying sizes. This method is favoured for producing GUVs since only a few components (current source, circuit and suspension well/vessel) are needed to obtain vesicles in a short time.[46]

One aspect which has yet to be shown is the merging or encapsulation of MOFs with in vesicles (rather than on to the vesicle membranes) to make a single biocompatible system which could potentially be used as a rapid delivery system or as a chemical/toxic removal system.

1.4 Project Aims

This project aims to investigate the uptake of sterols by a new β-CD porous network. If cholesterol, or structures of similar importance such as hormones or medicinal compounds, can successfully be bounded to a new porous β-CD network, or if MOF crystals could be encapsulated within vesicles then this could open up a new field of research in solid state chemistry. If successful, this could lead to the utilisation of solid-state materials within biological systems including but not limited to, transport of essential materials, removal of toxins or hazards, direct-to-cell drug delivery, specific cell to cell interactions, direct-to-cell cancer therapies, etc.

In this project new frameworks of β-CD with potassium were synthesised and analysed using different analytical tools and techniques such as X-ray diffraction, NMR spectroscopy and electron & optical microscopy.

2. Experimental

All chemicals and solvents were purchased from Alfa Aesar, Fisher Scientific, Sigma-Aldrich, Cambridge Isotope Laboratory and Avanti Polar Lipids and used without further purification unless stated otherwise.

Powder X-Ray Diffraction (PXRD): PXRD measurements were carried out at 298 K using a Rigaku benchtop X-ray diffractometer (λ (CuKα) = 1.5405 Å) on a zero-background holder. Data were collected over the range 3–45°. (University of Kent)

Single Crystal X-Ray Diffraction (SCXRD): A suitable crystal of each compound was selected and mounted on a Rigaku Oxford Diffraction Supernova diffractometer. Data were collected using Cu Kα radiation to a maximum resolution of 0.84 Å. Each crystal was kept at 100(1) K during data collection using an Oxford Cryosystems 800-series Cryostream. The structures were solved with the ShelXT[47] structure solution program using Direct Methods and refined with ShelXL[48] via Least Squares minimisation. Olex2[49] was used as an interface to all ShelX programs. The data was collected and solved by Dr Shepherd (Tables 2-4).

Thermal Gravimetric Analysis (TGA): Measurements were carried out using a NETZSCH STA 409 PC/PG apparatus. Measurements were collected from room temperature to 450 °C with a heating rate of 10 °C/min under an air atmosphere. (University of Kent)

Nuclear Magnetic Resonance Spectroscopy (NMR): NMR spectra were recorded on a JOEL NMR 400 MHz spectrometer and referenced to residual solvent peaks. (University of Kent)

Fluorescence Imaging: Fluorescent images were recorded on Etaluma Lumascope 620 digital microscope. The blue LED excitation was a wavelength

range of 473-491 nm and emission wavelength was in the region of 502-561 nm. (University of Kent)

Scanning Electron Microscopy (SEM): SEM images were recorded on a Hitachi S3400 SEM. The electron beam was set to 20 kV. Back scatter and secondary electron images were captured using inca software. (University of Kent)

2.1 Crystal Synthesis

2.1.1 KβCD-MOF-1

The method used to make edible MOFs (Smaldone *et al.*)[25] was adapted to be used for β-cyclodextrin in place of γ-cyclodextrin. The scale of the process was adjusted to be compatible with available glassware in the laboratory.

β-cyclodextrin (0.5675 g, 0.5 mmol) and potassium hydroxide (KOH) (0.5610 g, 10 mmol) was added to a 10 mL volumetric flask and dissolved in de-ionised water (10 mL). Then 1 mL of this mixture was added to a 2 mL borosilicate sample vial. The 2 mL sample vial was placed in a 14 mL sample vial which contained 2.5 mL methanol. This system was sealed with a cap and set aside for crystal formation over a period of 6-7 days. This was repeated a further nine times to obtain ten samples in total. To perform post synthesis analysis, crystals were carefully washed with 2 × 1 mL of ethanol. Elemental analysis for $C_{168}H_{295}O_{152}K_9$ ($4\beta CD \cdot 9KOH \cdot 4H_2O$) calc: C: 39.43, H: 5.85, N: 0.0; found: C: 39.59, H: 5.69, N: 0.0.

2.1.2 KβCD-MOF-1-Chol

A stock solution of β-cyclodextrin (0.5675 g, 0.5 mmol) was made in de-ionised water (10 mL). Potassium hydroxide (0.1122 g, 2 mmol) was weighed into a 2 mL

borosilicate vial and 2 mL of the β-CD stock solution was added (forming the KβCD-MOF-1 aqueous mixture). Then 1 mL of this mixture was added to an NMR tube. Deionised water of 0.1 mL was added followed by 0.1 mL methanol to the mixture in the tube. Cholesterol (0.0128 g, 0.033 mmol) was added to 2 mL methanol and then 1 mL of this solution was carefully added to each of the NMR tubes. The tubes were sealed with a cap and set aside for crystal formation for 2-3 weeks.

2.1.3 β-Cyclodextrin control crystals

β-cyclodextrin (0.5675 g, 0.5 mmol) was dissolved in 10 mL of de-ionised water in a 10 mL volumetric flask. 1 mL of this solution was added to a 2 mL sample vial then the smaller 2 mL sample vial was placed in a larger 14 mL sample vial which contained 2.5 mL methanol. This system was sealed with a cap and set aside for crystal formation over a period of 1-2 days.

2.1.4 KβCD-MOF-2

Potassium benzoate (0.0080 g, 0.05 mmol) was weighed into a 2 mL sample vial and this was used in the place of potassium hydroxide (which was used to make KβCD-MOF-1 in section 2.1.1.) in a 1:1 mol ratio with β-cyclodextrin. Then 1 mL of β-CD solution (0.5675 g, 0.5 mmol in a 10 mL solution) was added to the 2 mL vial. The 2 mL sample vial was placed in a 14 mL sample vial which contained 2.5 mL methanol. This system was sealed with a cap and set aside for crystal formation over a period of 4-5 days.

2.2 Sterol Uptake by New β-CD Network

2.2.1 Sterol uptake and Proton NMR study

A stock solution of cholesterol (0.005 M) was made in ethanol; 2 mL was added to some crystals to see if any changes occurred. The control β-CD was also used as a comparison. Proton (^{1}H) NMR was used to determine the ratio of β-cyclodextrin to bound cholesterol (in the crystal).

The solvents used for NMR analysis were deuterated dimethyl sulfoxide-d_6 (DMSO-d_6) and deuterated methanol-d_4 (MeOD) from Cambridge Isotope Laboratory. The ratios of solvents used for analysis of all the crystal samples (pure and soaked with sterols) were 750 µL of DMSO-d_6 with 100 µL of MeOD.

Three other sterol compounds, β-estradiol, testosterone and deoxycholic acid were also used to investigate the uptake of the new KβCD-MOF-1. The sterol structures are shown in Figure 2-1. The ratios of solvents used for analysis of pure sterols were 750 µL of DMSO-d_6 with 10 µL of MeOD.

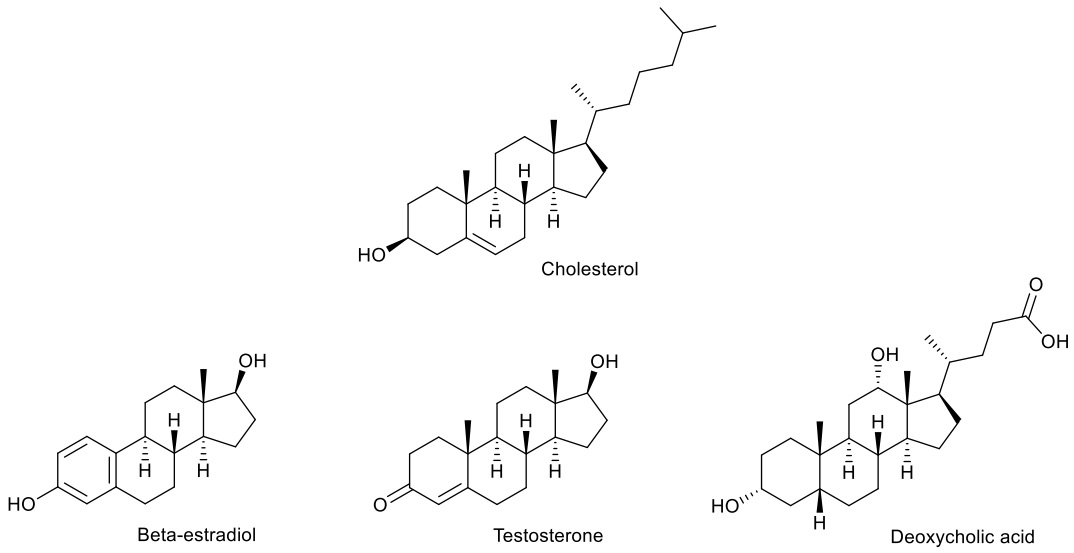

Figure 2-1: Structures of Cholesterol and other sterols used in this study

2.2.2 Imaging KβCD-MOF-1 soaked in topfluor cholesterol

A topfluor cholesterol solution was prepared by placing 50 µL of a 1mg/mL stock solution (Avanti polar lipids) into a 2 mL borosilicate sample vial. The chloroform was removed by drying the topfluor cholesterol under argon gas. Then 2 mL of ethanol was added to form a topfluor solution with a concentration 25 µg/mL.

Next the crystal samples of KβCD-MOF-1 were washed twice with 1 mL ethanol and then were transferred to a 10 mm microwell (35 mm diameter) petri dish.

The topfluor solution was carefully transferred to this petri dish and the dish was sealed with parafilm and set aside for duration of 24 hours.

After 24 hours, the parafilm was removed and the topfluor solution was extracted carefully. Then the crystal samples were immediately washed twice with 1 mL of ethanol and then 2 mL of ethanol was added to the petri dish for imaging the crystals in bright field and blue light excitation under an Etaluma Lumascope 620 digital fluorescence microscope.

2.3 Giant Unilamellar Vesicles

Giant unilamellar vesicle formation protocol was performed as described in Rossman *et al.*, Cell 2010.[50]

A lipid mixture was prepared by taking 40 µL of a 25 mg/mL stock solution of the lipid 1,2-ditetradecanoyl-*sn*-glycero-3-phosphocholine, DMPC (Avanti Polar Lipids), and 0.1 mol% TopFluor Cholesterol (Avanti Polar Lipids) was incorporated to form a mixture with concentration of 1 mg/mL in 1 mL chloroform.

Next the resistance across two indium-tin oxide coated slides (Delta Tech #CG-90IN-0115, 70-100Ω) surfaces were measured to determine which side of the slide was conducting. The uncoated side = large resistance reading (>1 MΩ), coated (conducting) side = small resistance (<1 kΩ).

A 9 mm Fastwell (Grace Bio, #664112) was placed on the edge of the slide on the non-conducting surface and a circular well area was marked, and then 6.5 µL of the lipid mixture was deposited onto the conductive side of an ITO coated slide (and repeated with a second slide).

The slides were dried in a vacuum chamber to drive off any excess chloroform (1-2 hours). To one of the slides a Fatwell spacer was placed over the lipid area to form a well and to this well 70 µL of an electroformation buffer (0.1 M sucrose, 1 mM HEPES) was added. The second slide was positioned, slightly offset, with the conductive side and lipids towards the spacer. The well was sealed by pressing both slides together as shown in figure 2-2. Copper taping was applied to the conductive side of the ITO slide and was used to form a complete circuit to a GW Instek SGF-1013 function generator. A voltmeter was added parallel to the slides.

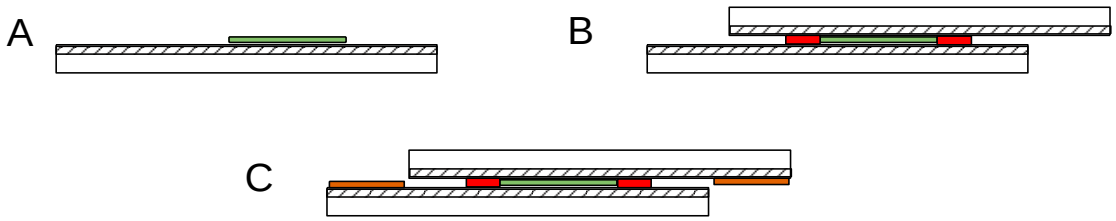

Figure 2-2: A) lipids (green) are thinly coated onto ITO slides, B) A pair of ITO slides are placed together with a fastwell spacer (red) with buffer to re-suspend lipids, C) copper tape (orange) is applied to the exposed conductive side of the ITO slides to be connected to a circuit with a function generator.

The GW Instek SGF-1013 generator was set to a sine wave of 10 Hz at 1.00 V for 4 hours and the slides were placed in a dark environment. After the 4 hours the circuit was dismantled and the slides were carefully taken apart. Approximately 60 µL of the samples (per pair of slides) was recovered using a wide bore pipette and added to an Eppendorf tube which contained 540 µL of a resuspension buffer (0.1 M glucose, 1 mM HEPES). About an hour before the electroformation was completed a Nunc Lab-Tek II chamber slide was opened and the wells were blocked with 5 % milk solution for an hour then this was washed with 3x phosphate buffered saline (PBS).

To view the vesicles approximately 200 µL of the re-suspended lipid mixture was carefully placed into the Nunc Lab-Tek II chamber slide wells. The chamber slide was placed onto an Etaluma Lumascope 620 fluorescence microscope and viewed under blue light excitation setting in a dark environment.

3. Results and Discussions

3.1 Cyclodextrin crystals

Cyclodextrins can easily form inclusion complexes with a variety of compounds and has been used in a wide range of applications in industry. More recently it has been demonstrated that cyclodextrins can be used to form biodegradable crystalline structures which themselves are able to form inclusion complexes.[25]

3.1.1 KβCD-MOF-1 network

MOF crystals were synthesised according to the vapour diffusion method outlined in section 2.1.1. The crystals were long 'needle-like' and white in colour. This new structure was named KβCD-MOF-1. The results from single crystal X-ray diffraction showed β-cyclodextrin channels which were perpendicularly stacked in layers with β-CD being held in place in the lattice by potassium (K) within the complex as shown in figure 3-1.

Also it was seen that the β-CD were arranged in primary to primary and secondary to secondary faces in the channel. The structure of CD-MOF-1 formed a cubic network with the secondary face forming the outer layers of the structure. The structure of CD-MOF-1 used a ratio of 8:1 K:γ-CD, this new KβCD-MOF-1 network used a ratio of 20:1 K:β-CD.

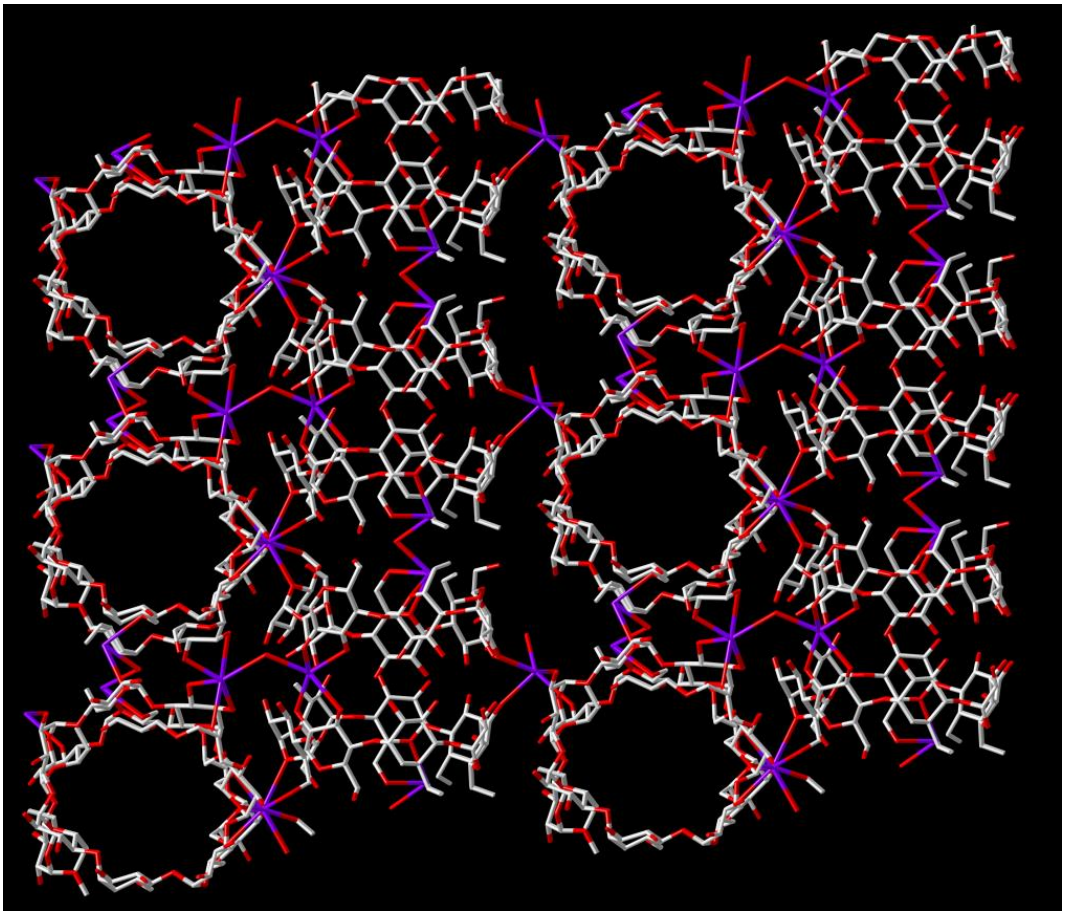

Figure 3-1: SC-XRD derived structure of KβCD-MOF-1, where white is carbon, red is oxygen and purple is potassium.

A previous structure incorporating β-CD, KOH and water was published in 1991 by Charpin *et al*.[51] The ratio they used to obtain a crystal was 1:1:8 of β-CD:KOH:water (Figure 3-2).

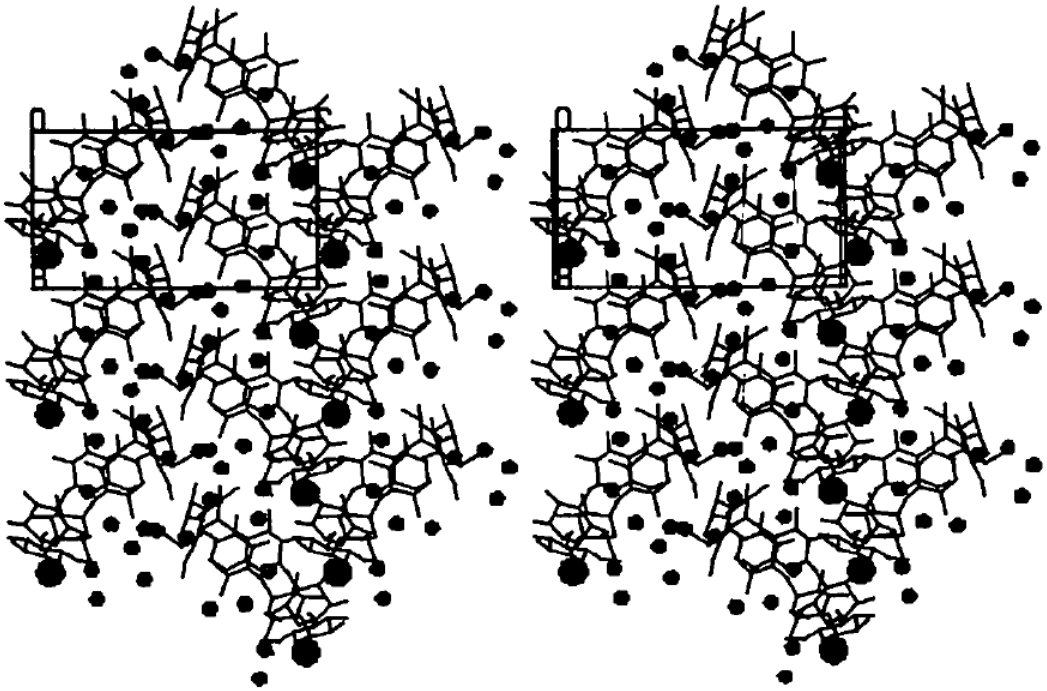

Figure 3-2: The herring bone scheme of the 1:1:8 β-CD:KOH:H_2O structure observed by Charpin *et al*.[51]

The structure they obtained was of cyclodextrins stacked in a herringbone scheme with potassium in between the lattice. Comparing the new KβCD-MOF-1 to the herringbone scheme, the similar features are that the new structure lattice is made of β-CD with potassium throughout the lattice holding the structure together. Where the structure by Charpin *et al.* had cyclodextrin stacked in an offset position (the cavities are not accessible), the new KβCD-MOF-1 was made of cyclodextrin channels (similar to nanotubes) stacked in perpendicular layers so all of the β-CD in KβCD-MOF-1 is fully accessible.

Another structure of β-CD was published in 1996 by Nicolis *et al*.[52] This structure was made of β-CD:calcium chloride:water in a ratio of 1:2:11.25 (Figure 3-3).

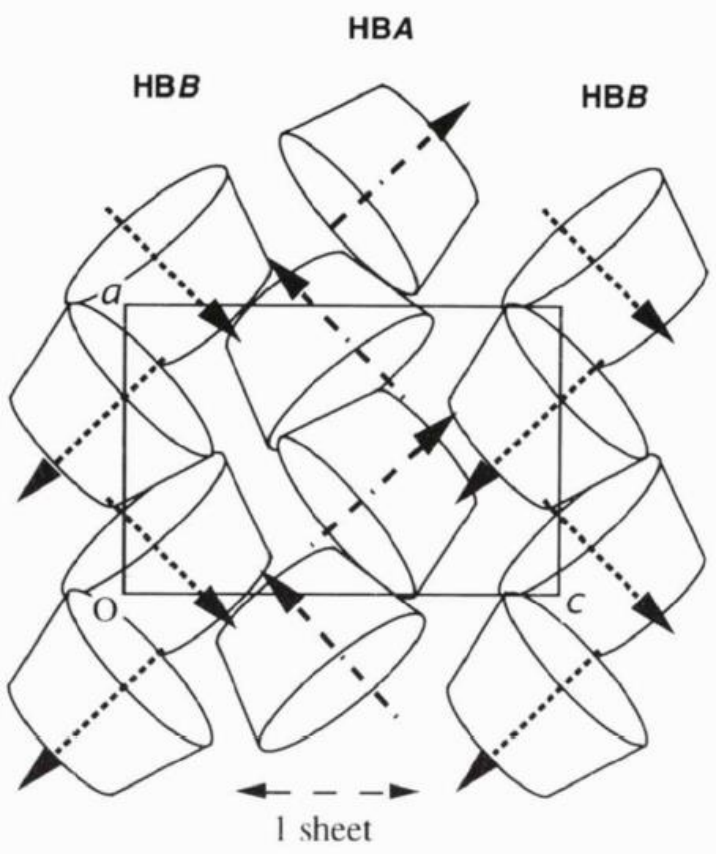

Figure 3-3: The herring bone scheme of the 1:2:11.25 βCD:$CaCl_2$:H_2O structure observed by Nicolis *et al*.[52]

Nicolis *et al*.[52] obtained a herringbone structure with both the calcium and chloride ions along with water molecules holding the lattice together crosslinking the cyclodextrin molecules. Therefore, with only water present as the main solvent the herringbone arrangement is the most stable for β-CD in a lattice. Unlike the structures observed by β-CD in water with KOH or $CaCl_2$ the new KβCD-MOF-1 was made in a water/methanol environment with a higher ratio of available potassium ions in solution.

CD-MOF-1 and CD-MOF-2 were made using exact ratio of available bonding site of γ-CD to potassium metal.[25,26] The vapour diffusion recrystallisation method used to synthesise γ-CD MOFs was adapted for β-CD and, in this project, the ratio of potassium metal was in excess to the number of available bonding sites per β-

CD molecule in a ratio of 20:1 potassium:β-CD. Upon recrystallisation by vapour diffusion, the 20:1 potassium:β-CD mixture produced a new crystal structure.

The lattice parameters for the new KβCD-MOF-1 crystal were a = 15.26(929) Å, b = 15.29(258) Å and c = 29.74(094) Å, α = 100.60(9)°, β = 94.36° and γ = 95.22(8)°. The spacegroup is Triclinic P1 (no. 1). The unit cell for KβCD-MOF-1 is K9CD4.

When the parameters were searched in CCDC database there were no other crystal structures with the above identity.

Thus, a new crystal network was identified using β-CD and potassium hydroxide.

3.1.2 β-Cyclodextrin control crystals

After the new β–CD networks were made and the method was established, a comparison was sought after to show that these structures were unique. Therefore vapour diffusion was carried out with only β-CD in water with methanol to see what would happen without the presence of any metals or other ions in solution.

When β-cyclodextrin was left to crystallise on its own, the large cubic crystals formed. These cubic crystals were analysed using SC-XRD (figure 3-4), showing that arrangement of β-CD a zipper, i.e. the β-CD cavities were blocked due to a staggered offset alignment of CD molecules.

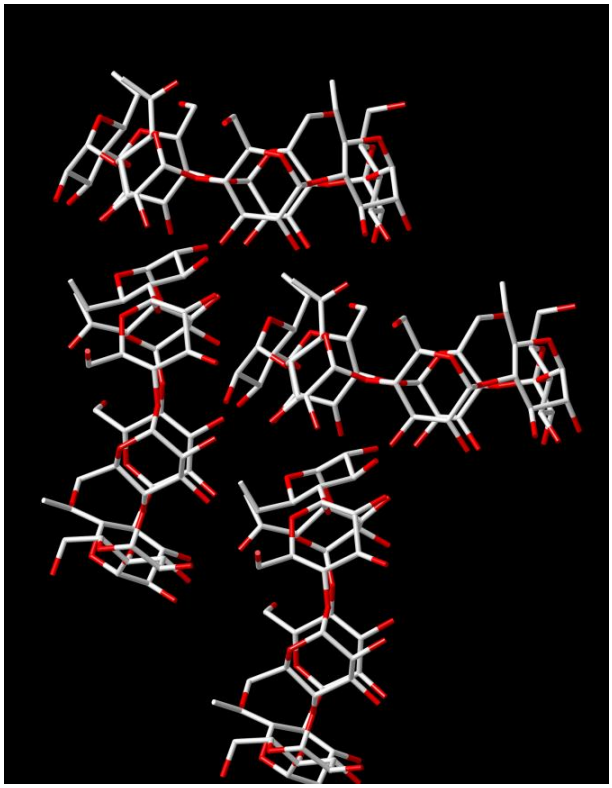

Figure 3-4: SC-XRD derived structure of control β-CD crystal, where white is carbon and red is oxygen.

Lattice parameters were a = 15.14(75) Å, b = 10.03(24) Å and c = 20.98(65) Å, β = 110.96°. The spacegroup was Monoclinic $P2_1$ (no. 4). The control crystals were held together by intramolecular forces between the cyclodextrin molecules such as hydrogen bonding between oxygen and hydrogen in the structures. The structure in figure 3-4 is similar to the herringbone structure by Charpin *et al.*[51] and Nicolis *et al.*[52] as the offset staggered arrangement of β-CD matches the herringbone scheme previously reported. Unlike those structures where the metal salts and water were present in between the cyclodextrin molecules, the control crystals formed in this project were made only in a mixture of water and methanol. This offset arrangement of β-CD means that beyond the outer layer of cyclodextrin the inner β-CD would not be accessible.

3.1.3 KβCD-MOF-2 network

Following the discovery of the β-CD KOH networks a different potassium salt (potassium benzoate) was used to see if that would have any effect on the crystal formation. Very fine small white coloured crystals were obtained from vapour diffusion. Figure 3-5 shows the structure of the CD-benzoate crystal analysed using single crystal X-ray diffraction. These crystals showed a 2D network of β-CD channels which were connected by potassium. Lattice parameters of KβCD-MOF-2 were a = 14.89(066) Å, b = 15.62(972) Å and c = 15.70(794) Å, α = 90.18°, β = 104.23(1)° and γ = 104.12(2)°. The spacegroup was *P1* (no. 1).

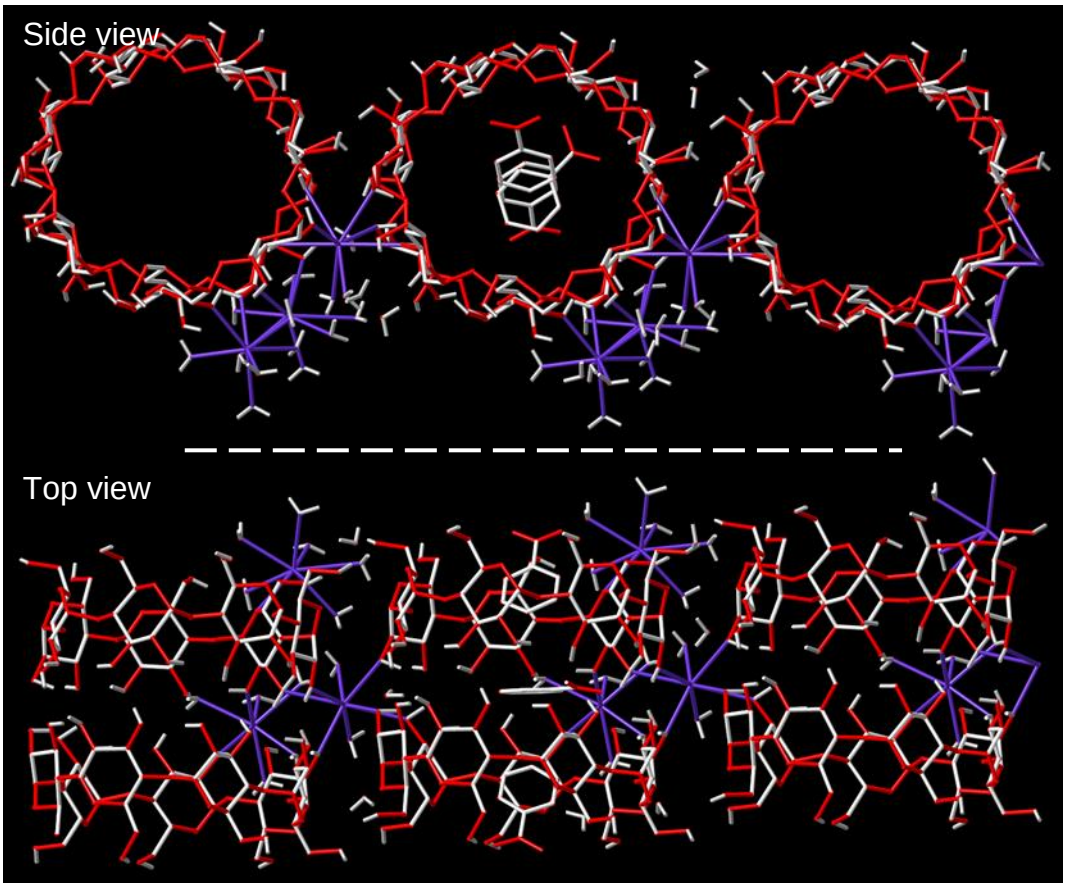

Figure 3-5: SC-XRD derived structure of KβCD-MOF-2 network, where white is carbon, red is oxygen and purple is potassium.

Within the pores of cyclodextrin, benzoate molecules were observed. Similarly to KβCD-MOF-1, the arrangements of β-CD molecules in this structure were primary face, secondary face, secondary face, primary face.

This structure was found to be similar to the benzoate inclusion complex with ratio of 2:2:0.7:20.65 β-CD:benzoic acid:ethanol:H_2O inclusion complex made by Thammarat Aree and Narongsak Chaichit, who also had a *P1* spacegroup.[53] They had obtained a lattice parameter of a = 15.210(1) Å, b = 15.678(1) Å and c = 15.687(1) Å, α = 89.13(1)°, β = 74.64(1)° and γ = 76.40(1)°. The crystal packing image is shown in figure 3-6. The main difference other than size was the angles determined for KβCD-MOF-2 was much greater than the inclusion complex alone.

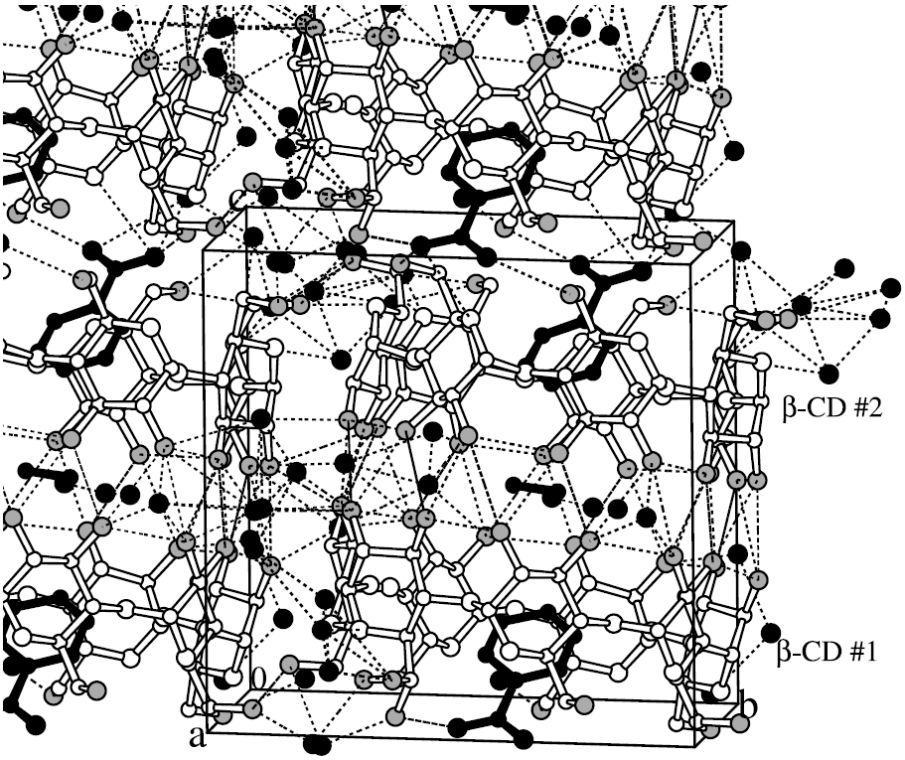

Figure 3-6: The crystal packing image of the 2:2:0.7:20.65 βCD:BA:C_2H_5OH:H_2O inclusion complex observed by Aree and Chaichit.[53]

The other difference between KβCD-MOF-2 and βCD-benzoate complex was that the inclusion complex was made by solvent evaporation in a water/ethanol mixture (after being heater to 60°C for one hour), whereas the KβCD-MOF-2 network was made by the vapour diffusion of methanol into an aqueous solution of β-CD and potassium benzoate at room temperature. As with the findings of Aree and Chaichit,[53] the benzoate molecules found in the central cavities of β-CD in KβCD-MOF-2 are also arranged so that the OH group points towards the primary face (shorter end of the cone). Three benzoate molecules are present in KβCD-MOF-2, these are shown in figure 3-5. The first and third benzoate molecules can be seen in the middle of the cyclodextrin cavities whist the second benzoate molecule is found parallel to the secondary face of β-CD. As benzoate molecules were observed within the cavities of the β-CD in this structure this showed that the β-CD of KβCD-MOF-2 are similarly accessible just like KβCD-MOF-1 network.

3.1.4 KβCD-MOF-1-Chol

The compound β-CD is in use today as a modulator of cholesterol concentration as described in section 1.3. Following the discovery of the KβCD-MOF-1 network by vapour diffusion, cholesterol was added to the crystallisation mixture of solvent diffusion to see if that would have any effect on the crystal formation of the KβCD-MOF-1 mixture. Figure 3-7 shows the structure of the β-CD-KOH-cholesterol crystal analysed using single crystal X-ray diffraction. This crystal showed a 2D network of β-CD channels which formed a honeycomb like structure which was different to both KβCD-MOF-1 and KβCD-MOF-2.

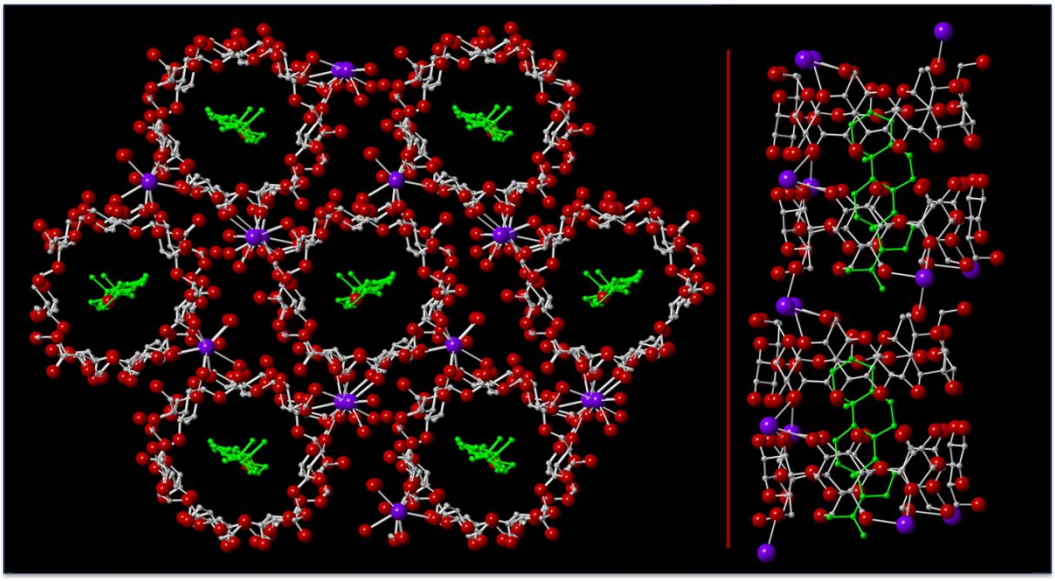

Figure 3-7: SC-XRD derived structure of KβCD-MOF-1-Chol network, where white is carbon, red is oxygen and purple is potassium.

On further analysis of KβCD-MOF-1-chol SC-XRD, it was found that cholesterol had partial occupancy of cyclodextrin (1 cholesterol molecule was observed for every 6 β-CD molecules in the lattice). The aliphatic chain (of cholesterol) was omitted from the SC-XRD image above due to a high degree of disorder in that part of the molecule. Comparing the crystal structures of KβCD-MOF-1 and that of KβCD-MOF-1-Chol the similarities are both used the same quantities of β-CD and KOH. The addition of cholesterol into methanol using solvent diffusion method formed a honeycomb like network rather than a series of perpendicular layered channels which were formed during vapour diffusion. The β-CD channels formed in KβCD-MOF-1-Chol similarly to KβCD-MOF-1 and KβCD-MOF-2 are accessible and here it was observed that cholesterol can be held within the β-CD cavity of this structure.

3.2 Powder X-ray Diffraction

Powder X-ray diffraction (PXRD) was used to initially assess the structure of bulk samples of the KβCD-MOF-1 network. PXRD is an analytical technique which can

provide information on the unit cell dimensions of a crystal and this is also a rapid technique to obtain the phase identification of a crystal sample, as in the name the sample is typically crushed into a fine powder before being placed in a diffractometer for analysis.

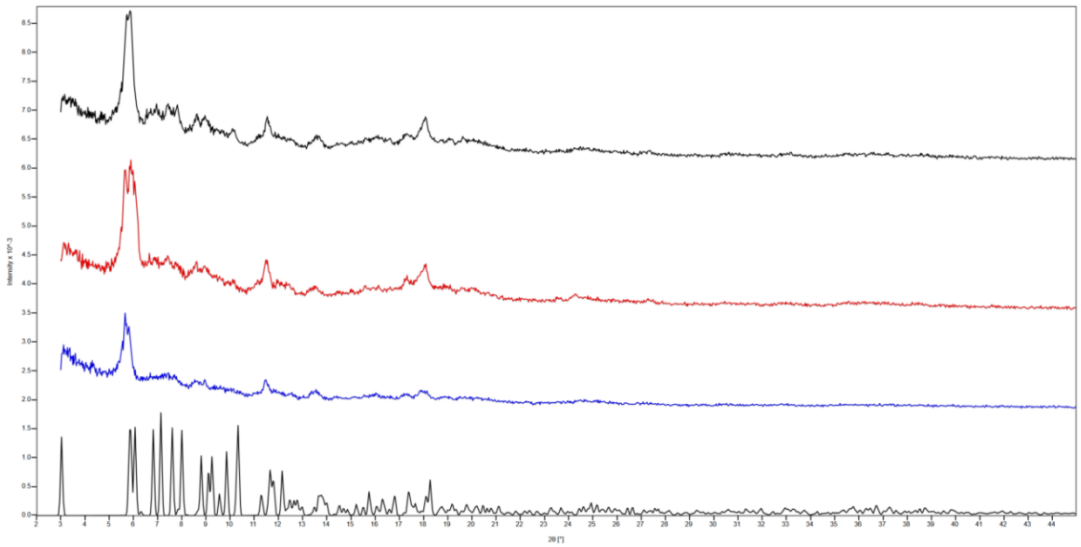

Figure 3-8: PXRD comparison of the KβCD-MOF-1 crystals, theoretical pattern from SC-XRD (bottom), initial experimental result (blue), KβCD-MOF-1 dried in vacuum (red) and KβCD-MOF-1 dried in air (top).

Figure 3-8 shows the PXRD patterns obtained for KβCD-MOF-1 experimentally and a predicted model which was based on the SCXRD structure of KβCD-MOF-1 crystal. Broad intensities (peaks) were observed in the experimental crystal patterns at values of 2θ at 6°, 11.5°, 13.5°, 17.5° and 18.2°. The positions of these peaks did match with the peaks in the predicted pattern. There were suggestions of peaks between 6-11° and 14-17° in the experimental patterns compared to the predicted pattern; however these could not be identified. Particle size is inversely proportional to peak width observed in XRD patterns.[54] Therefore the broadening seen in the experimental patterns could be due to small particles already present or which were formed when crystal samples were prepared for PXRD.

3.3 Cholesterol Uptake By New β-CD Network

The crystal structure of the KβCD-MOF-1 network showed continuous channels which closely resembled carbon nanotubes. β-cyclodextrin is known to effectively bind nonpolar molecules and methyl-β-CD has been shown to bind cholesterol.

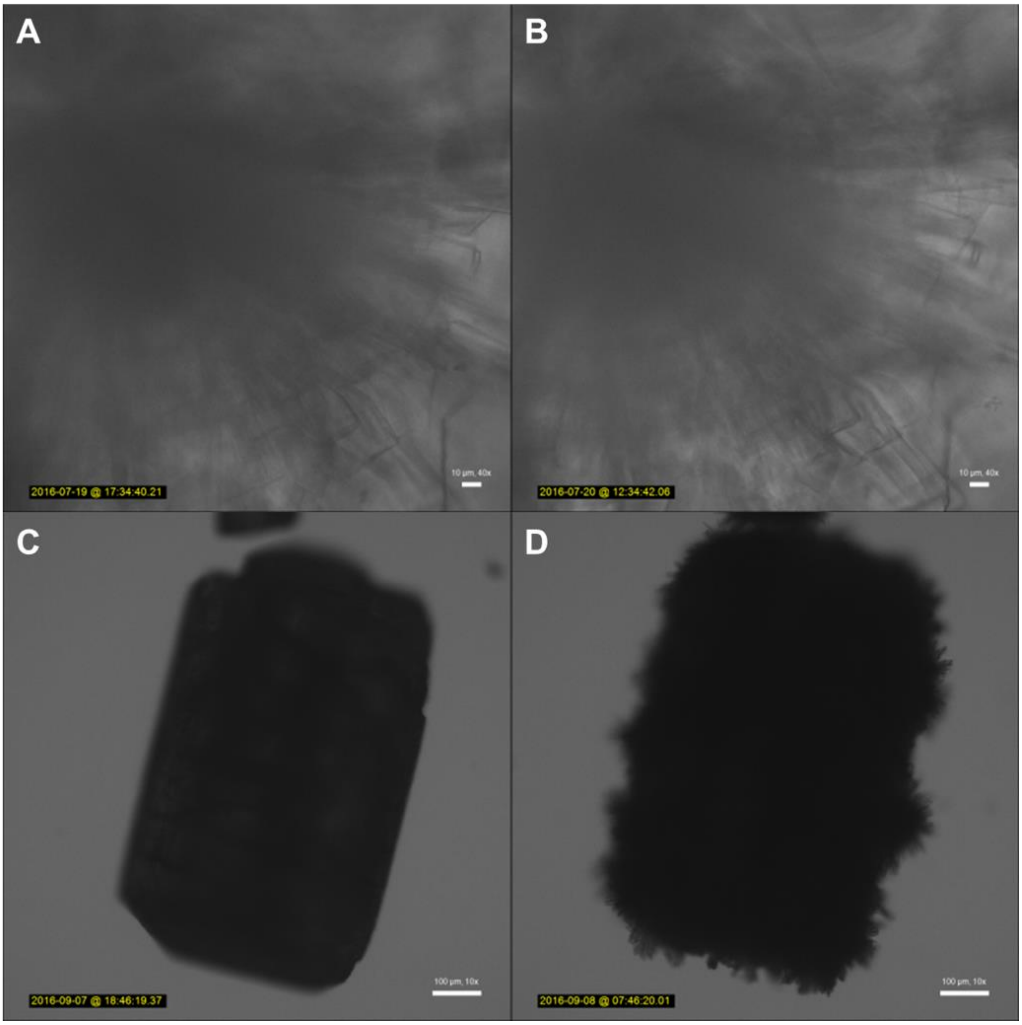

Figure 3-9: Images of KβCD-MOF-1 crystal before (A) and after (B) soaking in cholesterol solution, and images of β-CD crystal before (C) and after (D) soaking in cholesterol solution. The scale bar for A and B are 10 μm at 40x magnification and for C and D are 100 μm at 10x magnification.

It was decided to see if any interactions would occur between cholesterol in solution with the newly formed KβCD-MOF-1 network. Initially a stock solution of cholesterol (0.005 M) was made in ethanol; 2 mL was added to some crystals

(which were washed twice with 1 mL ethanol) to see if any changes occurred to the crystal morphology. The control β-CD was also used as a comparison.

The results showed that after an overnight soaking the morphology of the KβCD-MOF-1 ‘nanotube network’ crystals remained unchanged before and after soaking, this can be seen on bottom right hand side of figure 3-9 A and B. On the other hand the control crystal had additional crystal growth on the edges of the crystal after soaking, shown in figure 3-9 C and D, this was due to nucleation of cholesterol due to the inaccessibility to the cyclodextrin cavities in inner parts of the control crystal.

This showed the new KβCD-MOF-1 network was capable of up taking cholesterol without changing morphology. Therefore, KβCD-MOF-1 network could be used as a possible storage medium or adsorption medium for compounds such as cholesterol which plays a key role in the fluidity of cell membranes as described in section 1.4.

3.3.1 Uptake ratio determination using Proton NMR

In order to obtain a quantitative measurement proton (^{1}H) NMR was used to analyse the ratio of cyclodextrin to cholesterol up taken after soaking a sample of crystals in a known concentration of cholesterol (2 mL of 0.01 M) solution for 24 hours. The ratio was determined by using the integration of known distinctive functional groups on the respective compounds.

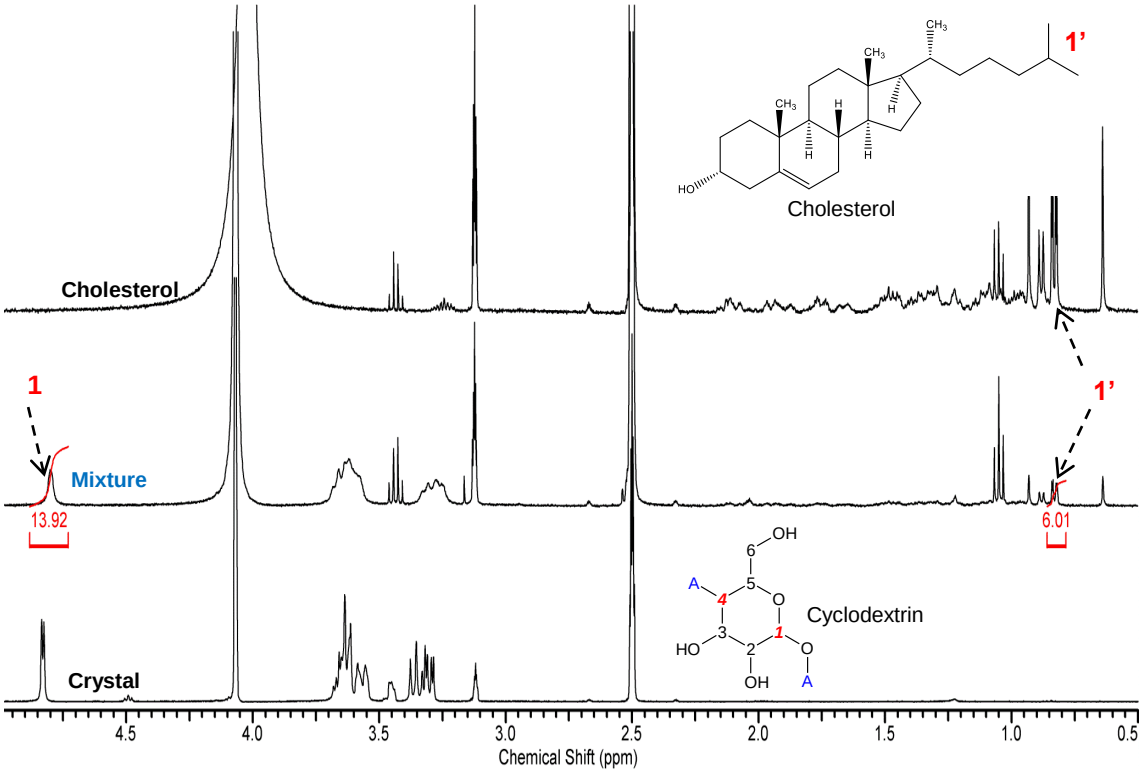

Figure 3-10: NMR Spectrum of cholesterol (top), KβCD-MOF-1 soaked with cholesterol (middle) and KβCD-MOF-1 crystal (bottom).

In order to compare the ratio of cyclodextrin to sterol present in the crystals certain peaks were chosen that were unique to respective molecule which would not overlap with the other structure. For β-cyclodextrin this was the glycosidic proton, since each β-CD molecule has a total of 7 glycosidic protons, the chemical shift occurred at 4.8 ppm.[55] In each case for individual sterols the pure spectra were compared to β-CD and peaks were chosen which could be distinguished as the sterols. For cholesterol the isopropyl group, at 0.8 ppm (**1'**) shown in figure 3-10, was chosen as it was known that the signal was due to the presence of 6 protons[56] therefore, by setting the integration at 0.8 ppm to 6, the ratio of β-CD to cholesterol was determined. The ratio was 13.92:6, i.e. 14:6, hence for every cholesterol molecule there were 2 molecules of cyclodextrin. In the KβCD-MOF-1-chol network it was observed that cholesterol partially occupied β-CD channels in

a ratio of 1 cholesterol to 6 cyclodextrin molecules and here similarly for every 2 β-CD, 1 cholesterol molecule was present.

3.3.2 Sterol uptake by new β-CD network

Three other sterol compounds, β-estradiol, testosterone and deoxycholic acid were also used to investigate the capability of the new KβCD-MOF-1 network. All three compounds shared the similarity of the sterol skeleton, however differed in the functional groups present in the structure as shown in figure 3-11.

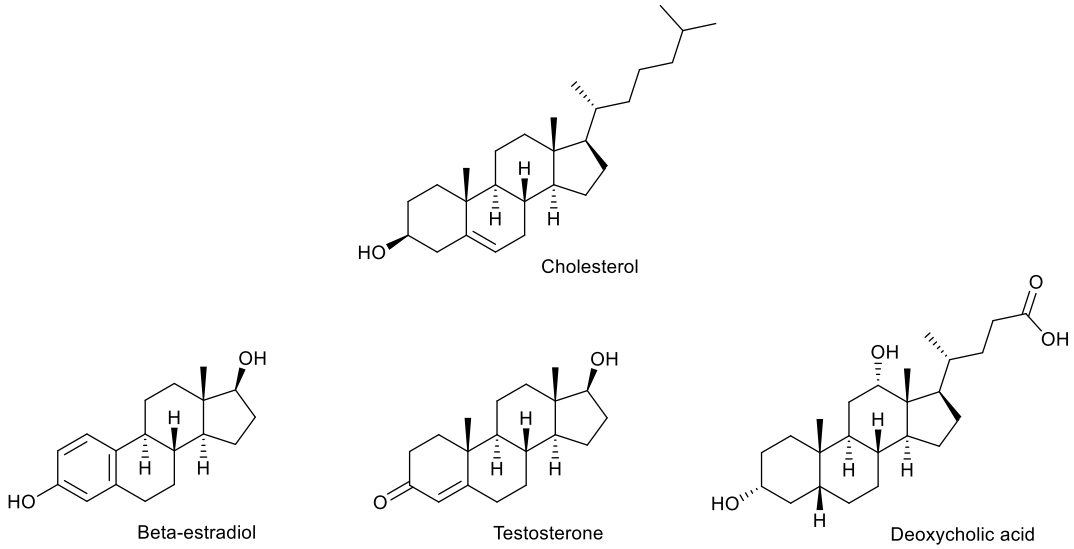

Figure 3-11: Structures of cholesterol and other sterols used in this study.

To see if any binding occurred between the KβCD-MOF-1 crystal and the other sterols, ^{1}H NMR was again used to analyse the ratio of cyclodextrin to sterol up taken after soaking a sample of crystals in a known concentration (2 mL of 0.01 M) of sterol solution for 24 hours respectively.

3.3.3 KβCD-MOF-1:Testosterone

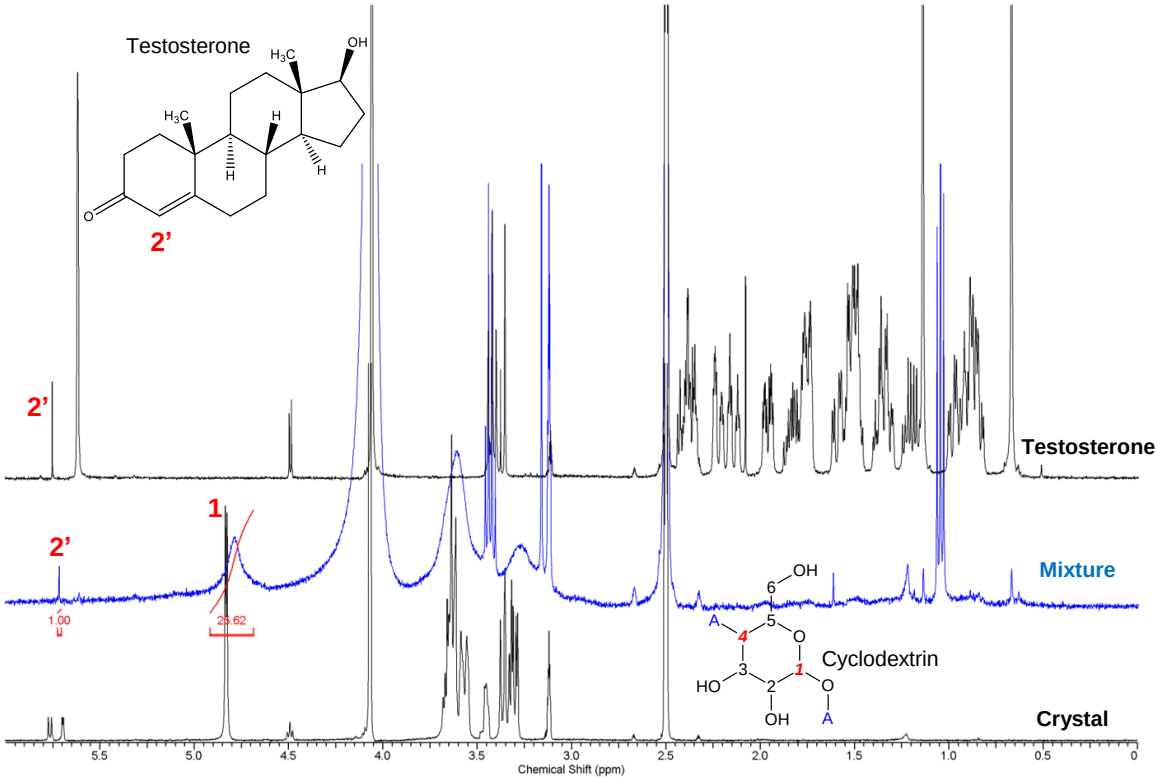

Figure 3-12: NMR Spectrum of testosterone (top), KβCD-MOF-1 soaked with testosterone (middle) and KβCD-MOF-1 crystal (bottom).

Similarly to cholesterol, for testosterone a proton environment was chosen which was unique to this structure shown in figure 3-12. The proton adjacent to the ketone group bonded to the unsaturated carbon (**2'**).[57] This was given integration of 1 at 5.7 ppm and then the glycosidic proton integration was determined. The ratio was 1:26.6 i.e. 1:27 which approximates to one testosterone to four cyclodextrin molecules. The peaks in the region of 3.0-3.75 ppm were broad due to high abundance of protons which could not be distinguished. The peaks for testosterone in the region of 0.5-2.5 ppm were not seen in the spectra of the mixture; this could have due to the protons of the testosterone hydrogen bonding to cyclodextrin cavity and hence be shielded. The peaks at 5.75 ppm in the crystal spectra were not present in the composite spectra as these were due to the hydroxide groups at carbons 2 and 3 on the cyclodextrin molecule.

3.3.4 KβCD-MOF-1:β-estradiol

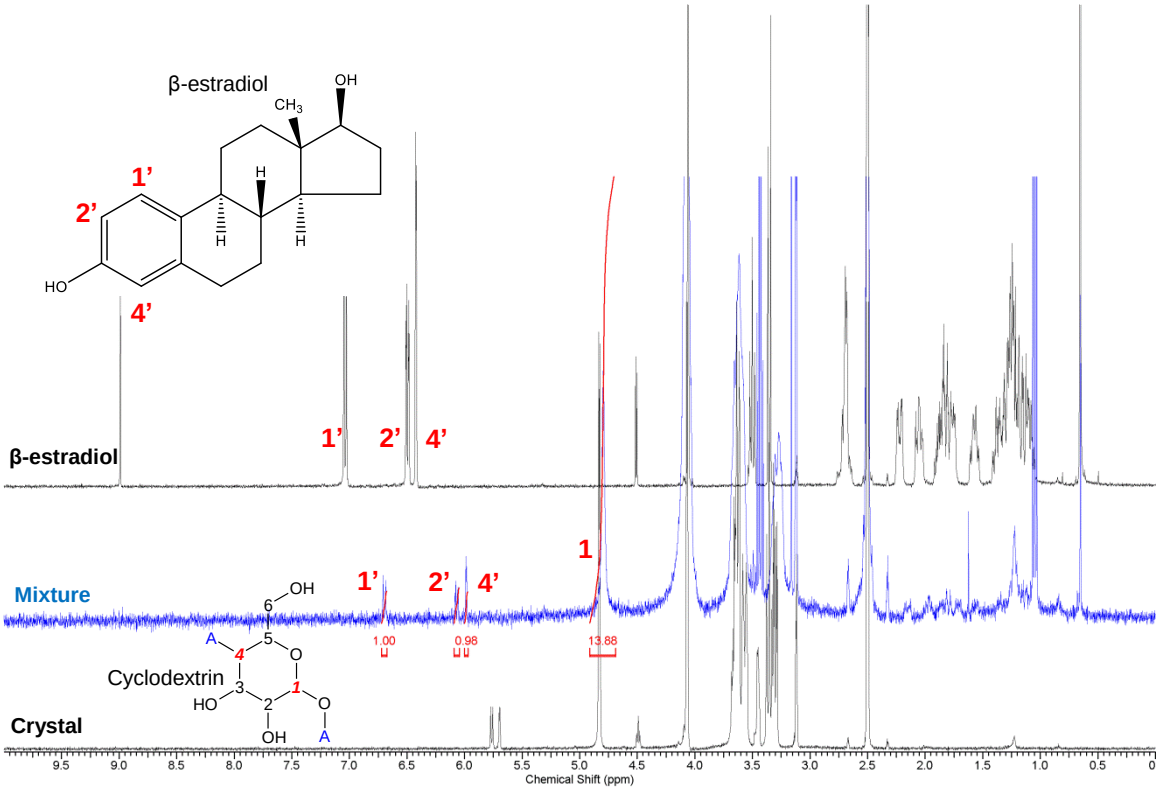

Figure 3-13: NMR Spectrum of beta-estradiol (top), KβCD-MOF-1 soaked with β-estradiol (middle) and KβCD-MOF-1 crystal (bottom).

Compared to the other sterols used in this study β-estradiol contained an aromatic tri-substituted benzene in the structure (**1', 2' and 4'**) shown in figure 3-13. Therefore, these unique protons were used to compare to β-CD which had no aromatic groups in the molecule. The chemical shifts of the aromatic protons occurred in the range of 5.98, 6.05, 6.70 ppm.[58] Hence as each of the aromatic protons produced integration of one, these sets of peaks were used as a comparison to β-CD. The ratio of β-CD to β-estradiol in figure 3-13 was 13.88:1, i.e. 14:1. For every one β-estradiol molecule there were 2 cyclodextrin molecules present. The down field shift of the aromatic protons in the composite spectra could be due to the hydrogen bonding of the β-estradiol to the β-CD cavity. The peaks at 5.75 ppm in the crystal spectra were not present in the composite spectra

as these were due to the hydroxide groups at carbons 2 and 3 on the cyclodextrin molecule.

3.3.5 KβCD-MOF-1:Deoxycholic acid

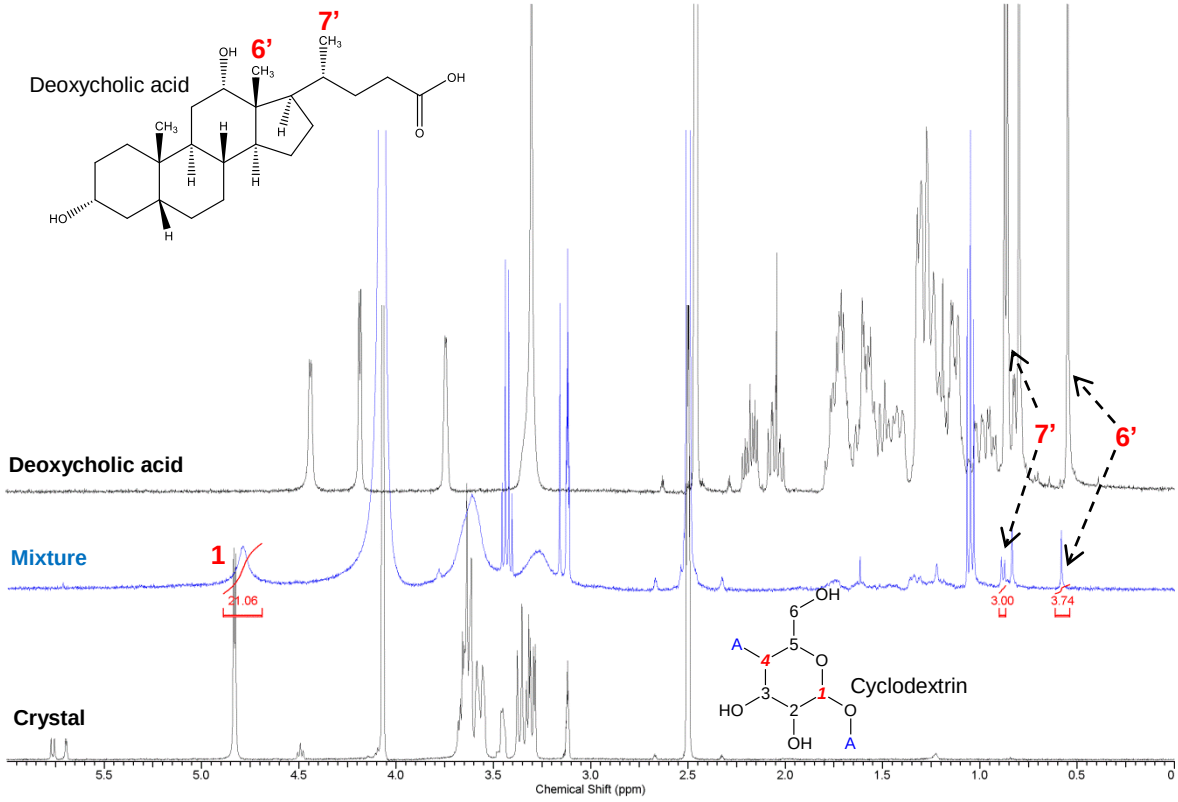

Figure 3-14: NMR Spectrum of Deoxycholic acid (top), KβCD-MOF-1 soaked with deoxycholic acid (middle) and KβCD-MOF-1 crystal (bottom).

The two relatively adjacent methyl groups on the alkyl chain (**6'**) and the cyclopentenyl group (**7'**), with chemical shift of 0.55 ppm and 0.85 ppm,[59] were selected for deoxycholic acid to compare with the glycosidic protons of cyclodextrin shown in figure 3-14. The ratio of cyclodextrin to deoxycholic acid was 21.06:3, i.e. 21:3. For every 1 deoxycholic acid there were 3 cyclodextrin molecules. Compared to cholesterol which has two hydrogen bonding sites at a hydroxide group and carbon-carbon double bond, deoxycholic acid has three areas for hydrogen bonding the two hydroxide groups and the carboxylic acid group at the end of the alkyl chain. The peaks at 5.75 ppm in the crystal spectra

were not present in the composite spectra as these were due to the hydroxide groups at carbons 2 and 3 on the cyclodextrin molecule. The signal broadening of the cyclodextrin peaks at 3.0-3.75 ppm and 4.75 ppm were due to the high abundance of protons which could not be distinguished.

The up field shift observed in the NMR spectrum of CD:sterols could be a result of hydrogen bonding between the sterols and β-CD molecule.[60] The inner cavity protons of β-CD (located at positions C3 and C5) have chemical shift values in the regions of 3.5 to 3.7 ppm in the NMR spectra in this section. In all of the mixture of β-CD and sterol spectra, the inner β-CD proton chemical shifts, as mentioned above, were not distinguishable due to broadened peaks which could be due to formation of inclusion complexes or exchange processes.[60]

The ratio of cholesterol to KβCD-MOF-1 crystal, shown in figure 3-10, was determined to be 1:2. Whist the crystal KβCD-MOF-1-Chol was found to have cholesterol occupancy of β-CD in a ratio of two β-CD molecules to one cholesterol molecule. Therefore it was concluded indirectly that the cholesterol being measured in figure 3-10 was bound to the inner channels of KβCD-MOF-1 crystals. As for the other sterols, with the available NMR data alone, it was difficult to conclude if the sterols being measured were not surface-bound to the KβCD-MOF-1 crystals because the peaks of interest for β-CD protons were indistinguishable due to peak broadening.

Table 1: Summary of NMR uptake studies

Sterol	Chemical Shift / ppm	Integration	Ratio of sterol:β-CD
Cholesterol	0.8	6.0	1:2
Testosterone	5.7	1.0	1:4
B-estradiol	5.98, 6.05, 6.70	0.98, 1.08, 1.00	1:2
Deoxycholic acid	0.55,0.85	3.7,3.0	1:3

The results summarised in table 1 obtained from the NMR uptake studies showed the new KβCD-MOF-1 network was able to uptake cholesterol and similar analogues of sterols. In section 3.1.4 KβCD-MOF-1-chol showed occupancy of cholesterol to be one cholesterol molecule per two molecules of β-CD. This was also confirmed by the NMR which showed 1:2 ratio of cholesterol:β-CD. The other sterols (testosterone, β-estradiol and deoxycholic acid) showed varying ratios to β-CD, after 24 hours of soaking. The ratio of testosterone, β-estradiol and deoxycholic acid to β-CD were 1:4, 1:2 and 1:3 respectively. The more electronegative functional groups present in the structure of the sterols the greater the ratio of β-CD:sterol. This indicates that the intake of the highly electronegative sterol was less than cholesterol as the number of β-CD per molecule increased. As the concentrations of the sterols were the same, testosterone and deoxycholic acid were taking up more space in the crystal pores compared to β-estradiol and cholesterol.

3.4 Thermogravimetric Analysis

Thermogravimetric analysis (TGA) was performed on KβCD-MOF-1 (Figures 3-15 and 3-16) to determine the thermal stabilities. Measurements were carried out under an air atmosphere, resulting in decomposition of the cyclodextrin occurring

from 250°C. Comparison of the samples, dried in two different methods, showed near identical loss of mass in the temperature range of 50-450°C.

Figure 3-15 shows the plotted data for the TGA analysis of the KβCD complex dried in air; here the loss in mass was recorded with respect to increase in temperature. The initial sample mass was 27.4 mg. As the temperature increased from 30-100°C a loss of 10% was observed and was due to loss of residual solvent within the crystals as the boiling points of methanol/ethanol/water were up to 100°C. A 50% mass loss was observed in the region of 220-320°C this was due to the thermal degradation of β-Cyclodextrin.[61]

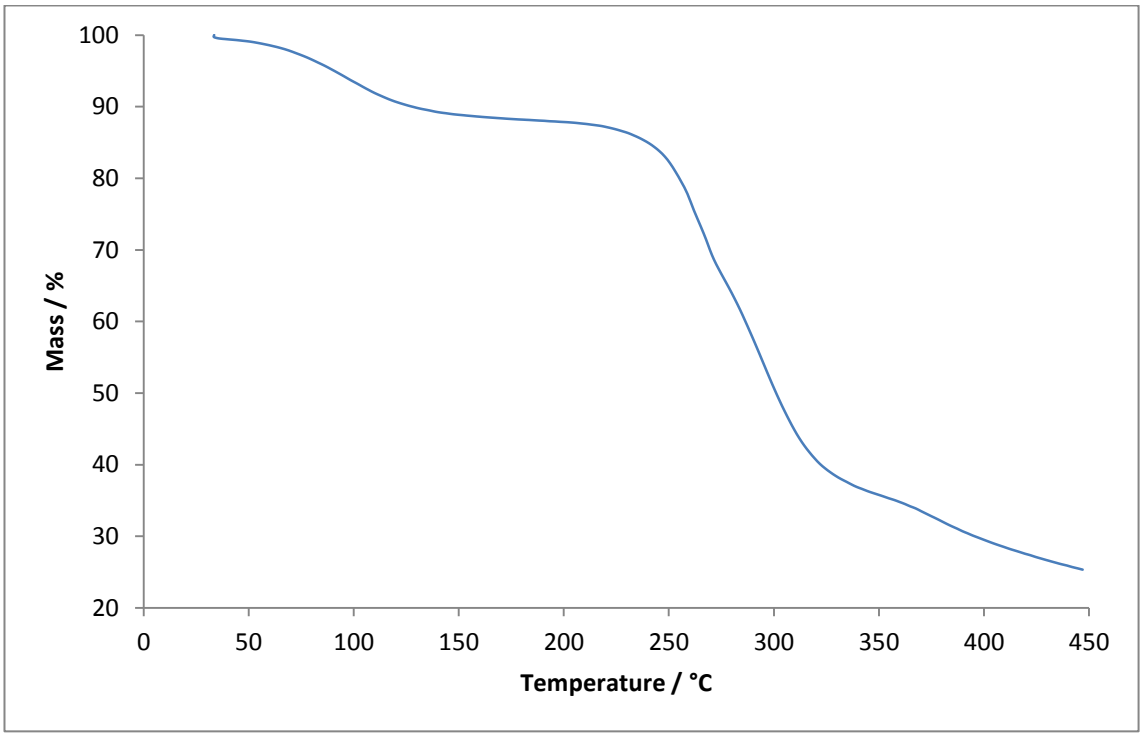

Figure 3-15: Thermogravimetric analysis of KβCD-MOF-1 network dried in air.

Figure 3-16 shows the plotted data for the TGA analysis of the KβCD complex dried in vacuum (using a schlenk line); here the loss in mass with respect to increase in temperature was recorded again. The initial sample mass was 8.1 mg. As the temperature increased from 30-100°C a loss of 10% was observed and

was due to loss of residual solvent within the crystals as the boiling points of methanol/ethanol/water were up to 100°C. A 50% mass loss was observed in the region of 220-320°C this was due to the thermal degradation of β-Cyclodextrin.[61]

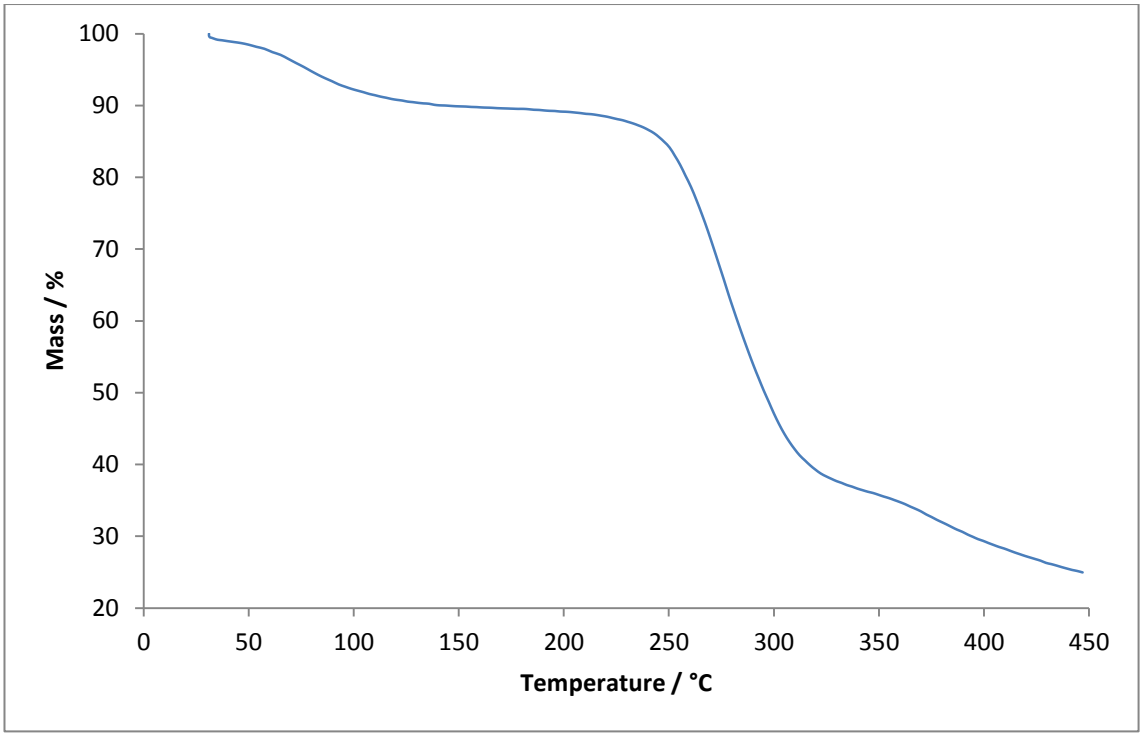

Figure 3-16: Thermogravimetric analysis of KβCD-MOF-1 network dried in vacuum.

Both of the thermogravimetric plots showed that the different methods of drying the crystal samples yielded very similar result even when the mass of sample used was different. This showed that due to the structure being made of layered β-CD nanotube channels some solvent was always retained within the crystal complex regardless of being dried in normal atmosphere or under vacuum pressure.

3.5 KβCD-MOF-1 Crystal Imaging Analysis

The KβCD-MOF-1 network have been observed by eye, by optical microscope to see shapes of the crystals that had formed and even analysed by X-ray diffraction to determine the structural arrangement of the molecules and atoms it was composed of. One aspect which was not initially considered was the surface topography of crystals. In order to see the crystal topography, a scanning electron microscope was used to obtain back scatter and secondary electron images of the crystals at a micrometre scale.

The following figures (3-17 to 3-20) show various images of KβCD-MOF-1 crystal. One significant aspect which was seen only with the use of SEM was that what appeared to be single long needle like crystals by eye was actually made up of a series of layered crystals similar to fallen dominoes. The latter two figures show clearly that the larger crystal structure began from a central area.

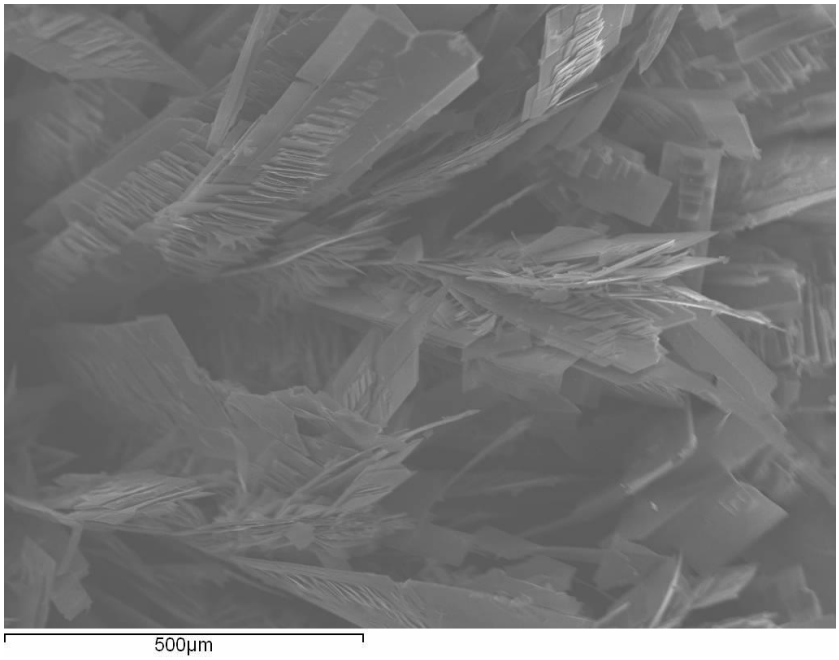

Figure 3-17: SEM image of KβCD-MOF-1 crystal showing long needle crystals was composed of additional layered addititions.

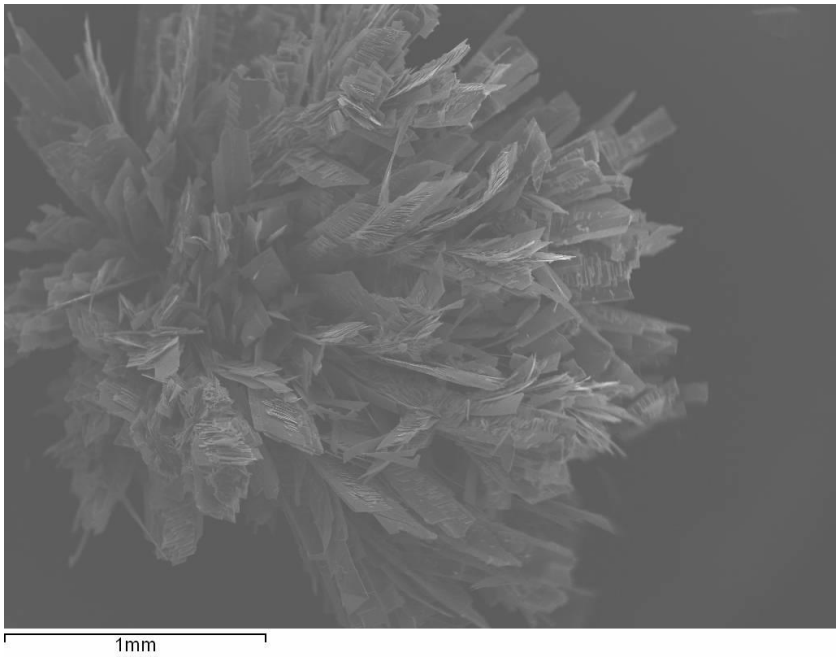

Figure 3-18: A full view of a KβCD-MOF-1 crystal (secondary electron image) again showing the whole of the crystal being composed of highly layered structures.

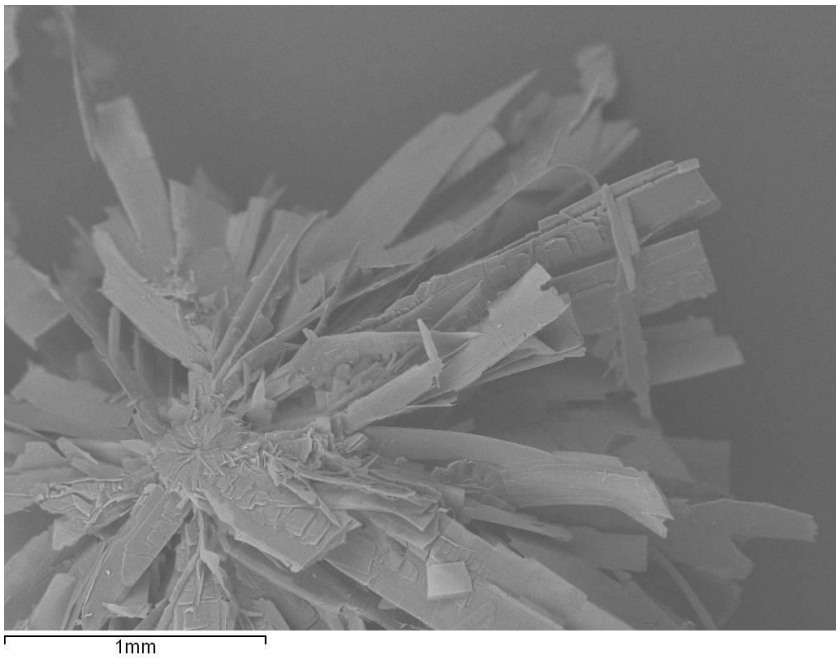

Figure 3-19: Back Scatter electron image of KβCD-MOF-1 crystal showing the point from which the crystal grew outwards, additionally layering of the crystal can be seen.

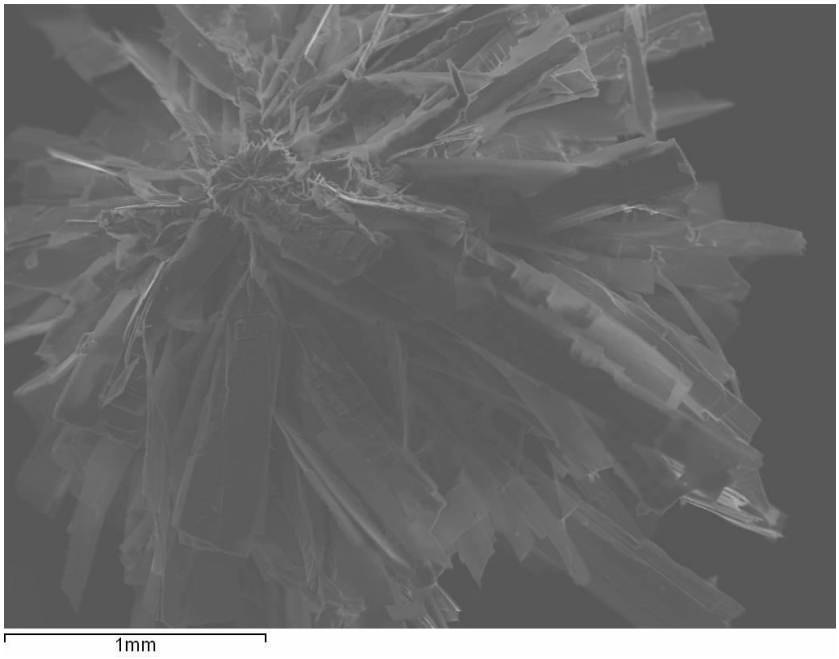

Figure 3-20: Secondary electron image of the nucleation point of the KβCD-MOF-1 crystal the topography can be seen clearly, a central mass of crystal initially formed then as the crystal was left to nucleate the starburst effect occurred in which layering of the needle strands can be seen.

3.5.1 Imaging KβCD-MOF-1 soaked in Topfluor cholesterol

It was observed that KβCD-MOF-1 network was able to be soaked in a solution of cholesterol over a 24 hour period without changing the crystal morphology. Additionally when KβCD-MOF-1 was made using solvent diffusion in the presence of cholesterol KβCD-MOF-1-chol was made. Both of these networks showed that the ratio of cholesterol:β-CD was 1:2. Therefore, topfluor cholesterol was used in a similar study to see what would happen to KβCD-MOF-1 after being soaked for 24 hour period.

After soaking KβCD-MOF-1 crystals in topfluor cholesterol images were taken in bright field and blue LED excitation, shown in figure 3-21, after being washed in ethanol. In blue fluorescence it was seen that the crystals were much brighter than

the surrounding medium which indicated that topfluor cholesterol was retained on the crystal.

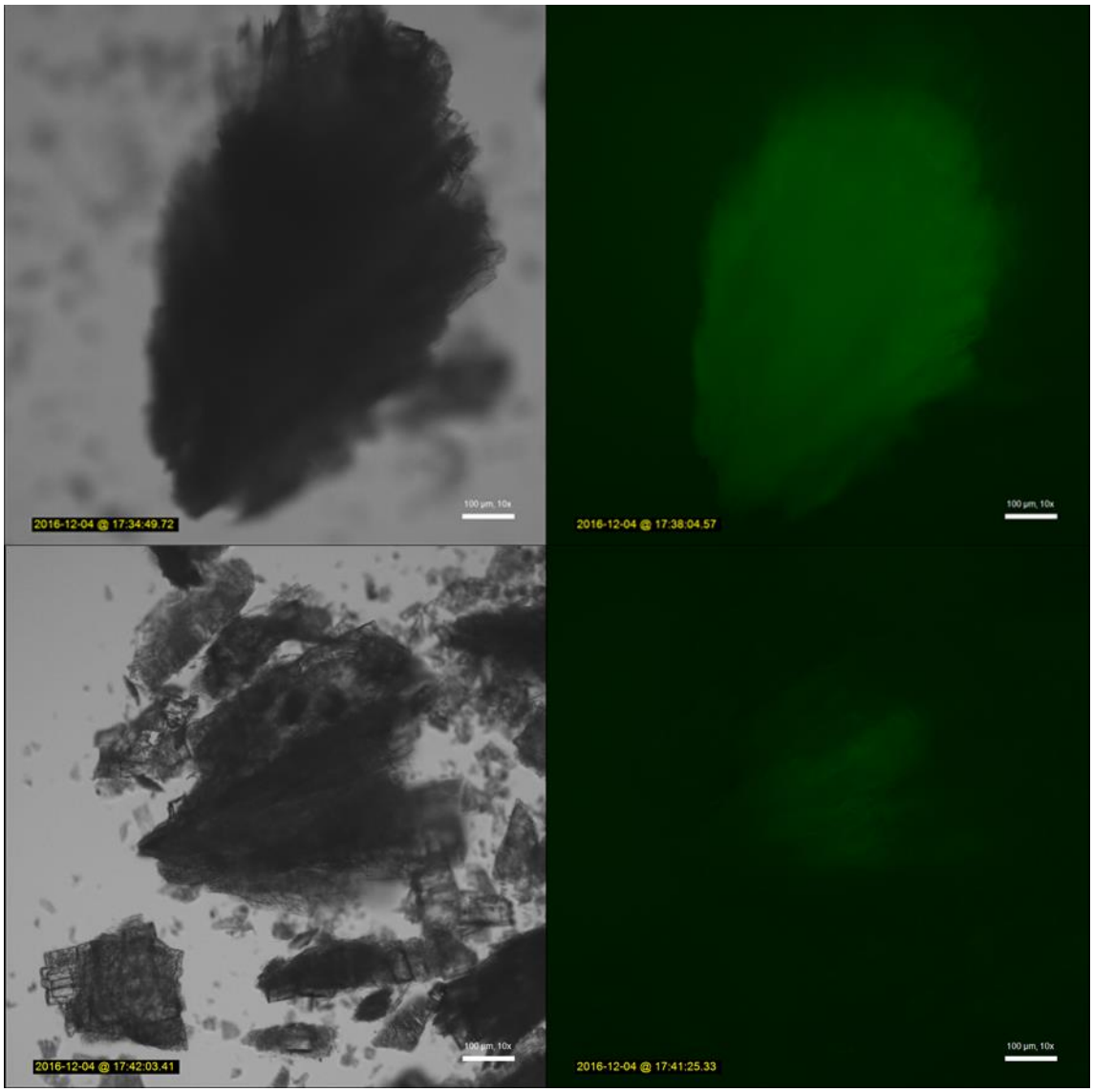

Figure 3-21: Images taken on the lumascope of KβCD-MOF-1 crystal which was washed twice using 1ml ethanol after being soaked in topfluor cholesterol for 24 hours (Left in bright field/white light and right in dark blue light). The scale bars on all 4 images are 100 μm at 10× magnification.

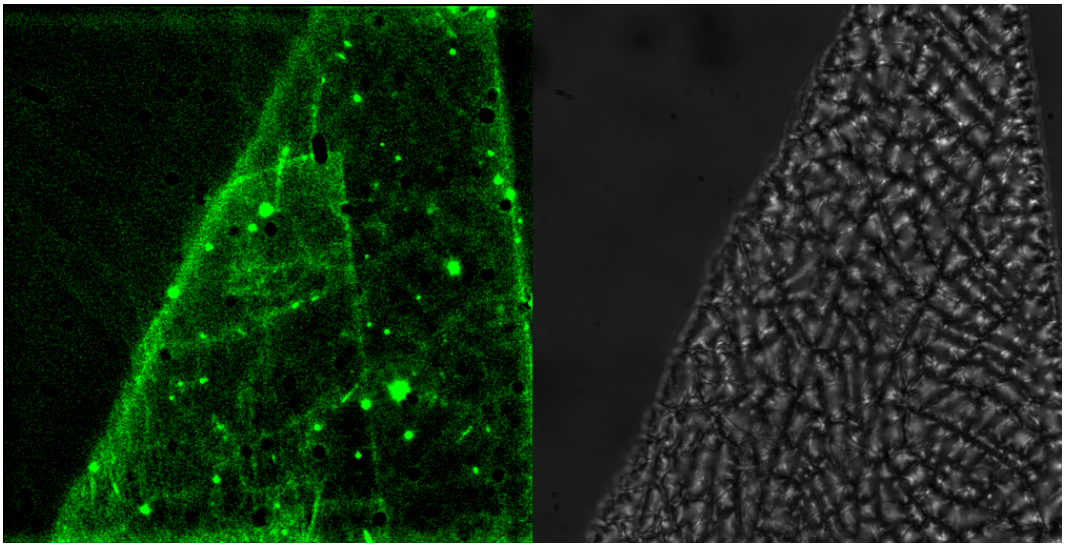

Figure 3-22: More detailed images of another KβCD-MOF-1 crystal which was washed twice using 1ml ethanol after being soaked in topfluor cholesterol for 24 hours (Left in blue light and right in brightfield/white light).

The results (figures 3-21 and 3-22) showed that KβCD-MOF-1 network in addition to up taking cholesterol was also able to retain topfluor cholesterol when soaked in solution. Both figures 3-21 and 3-22 show the surface of KβCD-MOF-1 crystal. In the latter case more surface details could be seen. The areas of high intensities in figure 3-22 represent higher concentration of topfluor in those areas. Additionally this top down view of the crystal showed more intense fluorescence along the edges of the crystal network.

The bright field image (right hand side of figure 3-22) shows what appears to be cracks or irregularities on the surface of the KβCD-MOF-1 crystal, this may have occurred due to exposure of the crystal to air, or even when washed with ethanol. The images taken after the soakings were in ethanol, it was seen that the fluorescent intensity decreased as more time went on. This, along with higher intensities at the edges of the crystal, suggested that topfluor cholesterol was binding to the surface of the crystals and ethanol was displacing the cholesterol after soaking.

Therefore, as topfluor cholesterol contained the bodipy group and normal cholesterol was shown to be up taken fully into β-CD cavity, mixtures of such compounds could be used as a potential method to induce a controlled uptake of similar compounds into the newly formed KβCD-MOF-1 network.

As described in section 1.3 these molecules have also been utilised in biosciences to visualise processes such changes in membrane curvature during viral budding.

3.6 Vesicles and encapsulation

Vesicles have been used in a wide range of studies, ranging from studies of membrane processes to acting as artificial cells used for drug delivery. Metal Organic Frameworks have also shown to be effective to be used in drug delivery. One aspect which has yet to be shown is the merging of both materials to make a biocompatible system which could potentially be used as a rapid delivery system or as a chemical/toxic removal system.

Figure 3-23 shows some images of vesicles made using 1,2-ditetradecanoyl-*sn*-glycero-3-phosphocholine (DMPC) lipid and topfluor cholesterol after the electroformation process taken on an Etaluma Lumascope 620 digital microscope made throughout the duration of this project. The excitation wavelength was in the range of 473-491 nm and emission wavelength was in the region of 502-561 nm. In the four images (figure 3-23) vesicles can were seen clearly in a dark environment using a blue LED source. The vesicles formed were random in size with some being 10μm and others were larger with additional vesicles inside. As described in section 1.3, electroformation is quick process and yields vesicles of various sizes this can be seen in figure 3-23. The areas of high fluorescent intensity are more intense in contrast to the surrounding medium, this indicates regions of highly concentrated topfluor cholesterol or where vesicles have

aggregated. The electroformation method used for making these vesicles showed that so long as an alternating current source was available, it was possible to make GUVs with readily available materials.

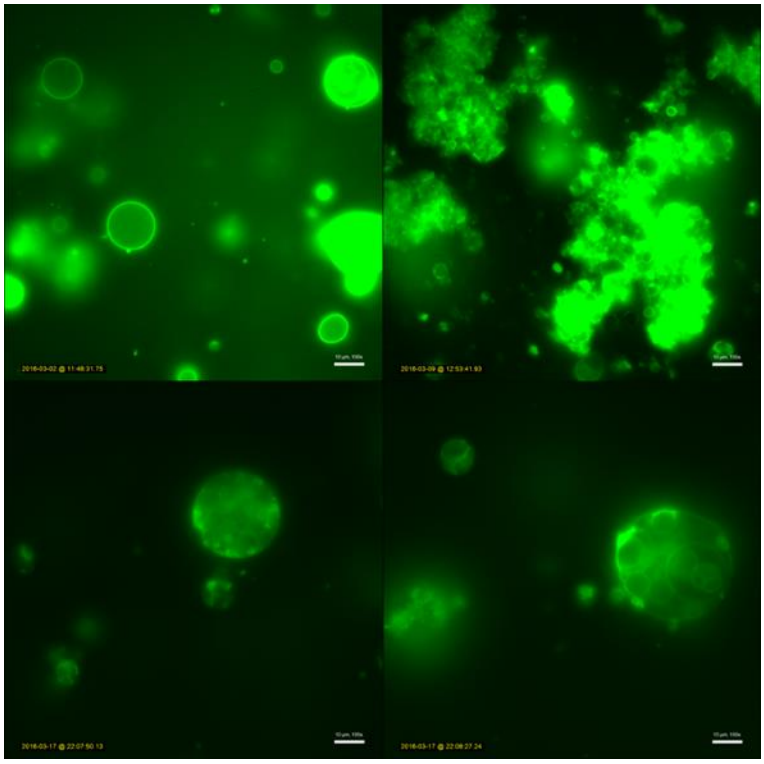

Figure 3-23: Various images of vesicles made using DMPC lipid with 0.1mol% incorporated topfluor cholesterol taken on the lumascope. The scale bars on the images are 10 µm at 100× magnification.

Previous to this study, there was no recorded literature which in MOFs had been encapsulated within vesicles. Therefore, using UiO-66 crystals made in the Blight group; encapsulation of UiO-66 was attempted to see if it would be possible to see both crystal and vesicle structures clearly.

A known MOF, UiO-66, was used to try to encapsulate into vesicles. This was done by adding UiO-66 to the electroformation buffer then using this in the stage of re-suspending lipids prior to electroformation. Initial viewing of the results under the lumascope (figure 3-24) showed that when viewed under bright field the UiO-

66 MOF crystals were clearly seen, whilst in blue light excitation the vesicles were seen to be surrounding the position of the crystal clusters.

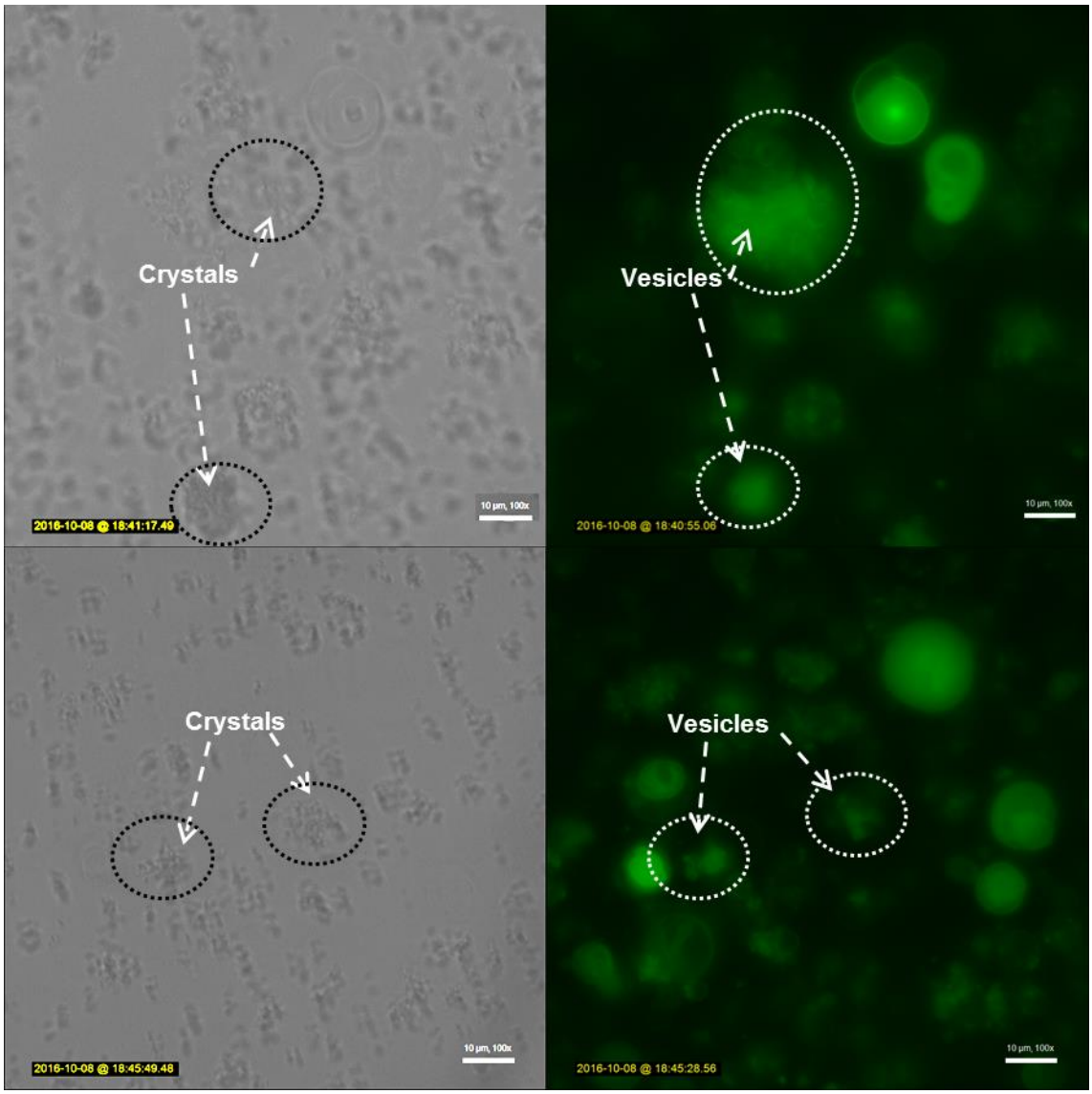

Figure 3-24: Brightfield image showing UiO-66 MOF crystals (left) and the same image in blue light excitation showing vesicles (right) taken after electroformation with UiO-66 MOF crystals present in solution. The scale bars on the images are 10 µm at 100× magnification

TEM was used to see if encapsulation of MOFs was successful. Preliminary image captured (Figure 3-25) showed that the crystals were clustered centrally because the arrangements of the crystals were circular. As the contrast is higher around the

circumference of the crystals it could be an indication that a membrane is surrounding the crystals. However there were no empty vesicles visible.

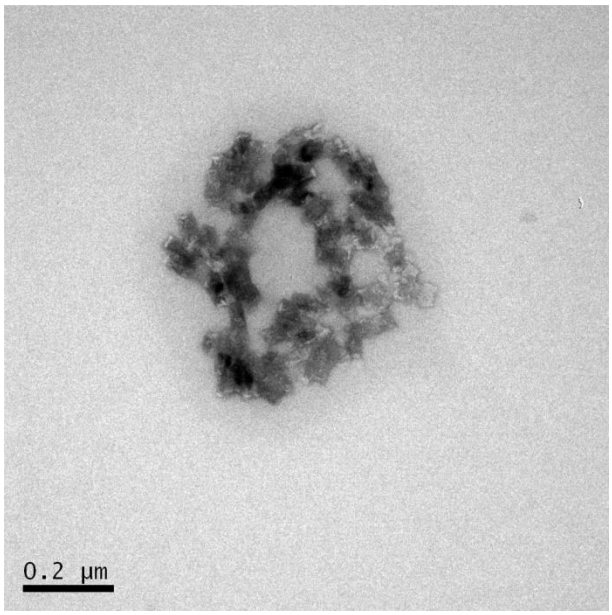

Figure 3-25: Preliminary TEM image of UiO-66 MOF crystals captured after encapsulation with in unilamellar vesicle.

Although from figure 3-24 there is an indication that encapsulation was there however from figure 3-25 it cannot be concluded conclusively if the encapsulation of UiO-66 with in vesicles had taken place. Additionally as far as our understanding was this was the first attempt to incorporate crystals inside vesicles rather than on the outer or inner surfaces of membranes.

Sometimes it is possible to get drying artefacts when preparing samples for TEM analysis.[62] These can occur during the sample preparation when dispersed samples are dried on a TEM grid but residual liquid is retained on the surfaces of samples of interest. This can lead to possible coffee ring effects wherein there could be dark patches around the perimeter of samples viewed under TEM. With only the image seen in figure 3-25, it was not possible to confirm if the dark perimeter around the crystal cluster was either a drying artefact or a vesicle membrane.

4. Conclusions and Future Work

4.1 Conclusions

Metal organic framework, as defined by IUPAC guidelines is a coordination network with organic ligands which contain potential voids.

A new beta-cyclodextrin-potassium network named KβCD-MOF-1 and two other analogues KβCD-MOF-1-Chol and KβCD-MOF-2 were made successfully. The crystal structures of the new network and other β-CD crystals were analysed by X-ray diffraction. The new 1:20 β-CD:K KβCD-MOF-1 crystal is made of layers of cyclodextrin channels which are stacked perpendicularly from one layer to the next. The control cyclodextrin crystals show a stacking formation by which the cavity of the cyclodextrin is inaccessible due to an offset arrangement of the β-CD. When cholesterol is added in the 1:20 mixture before crystal formation, a new crystal was formed named KβCD-MOF-1-Chol. This structure looked like a honeycomb and within the cavity of every 6 β-CD molecules 1 cholesterol molecule was observed. A 1:1 ratio of β-CD:potassium benzoate resulted in another structure named KβCD-MOF-2. This was similar to a previous inclusion complex but was unique due to the crystal lattice being made by solvent diffusion rather than solvent evaporation.

The morphologies of the control β-CD crystals and KβCD-MOF-1 crystals were tested by placing these into a solution of cholesterol in order to investigate any changes to the physical properties of the crystals; the former was seen to have nucleation of cholesterol on the edge of the structure after soaking, whilst the KβCD-MOF-1 crystals remained unchanged throughout the soaking. Hence the KβCD-MOF-1 crystal was able to be soaked in cholesterol without changes to the physical properties.

The uptake of cholesterol and several other sterols (testosterone, β-estradiol and deoxycholic acid) were performed on the newly formed KβCD-MOF-1 network by soaking the crystal in a solution of the respective sterol. The ratio of sterol:β-CD was determined using proton NMR analysis. The results were cholesterol:β-CD was 1:2, testosterone:β-CD was 1:4, β-estradiol:β-CD was 1:2 and dexoycholic acid:β-CD was 1:3. The results showed that uptake of these sterols were successful. The NMR results also showed an inverse relation between numbers of polar groups in the sterol to the uptake by KβCD-MOF-1 network.

The preliminary results obtained for the vesicle encapsulation study using UiO-66 crystals could not be concluded. The fluorescent and bright field images on the lumascope showed clusters of crystals in the same regions as vesicles. However additional testing will be required to conclusively confirm if the methods used for encapsulation of UiO-66 crystals with in vesicles had been completed.

4.2 Future work

The discovery of a new material, be it a crystal or otherwise, brings forth many new challenges to discover what it can do, how stable it could be in ambient conditions and what would happen in extreme conditions.

The greatest limitation to such a research project was time. With the time available in this project the decision was taken to investigate uptake of cholesterol and some other similar analogues with the sterol back-bone. To carry on with further analysis of the various crystals, the porosity could have been modelled using the crystal structure (theoretical) and then carried out using nitrogen adsorption (experimental) this would have provided data of how much of the internal volume of the network could be available. Uptake studies would have been carried out using a mixture of compounds (such as a mixture of cholesterol and estradiol) to

see if the crystal would either separate similar substances or if uptake would be favoured by one molecule over another. This in turn could be used to see if the β-CD networks could be used to isolate and remove specific molecules such as cholesterol or perhaps be used to separate mixtures which otherwise may need to be treated to isolate. Using compounds which have different dyes could also be used to determine if inclusion complexes of KβCD-MOF-1 can be used to uptake certain quantities of one molecule and then be capped by a second molecule. This would be beneficial in pharmaceuticals as a potential rapid drug delivery medium.

Ethanol was found to be the medium in which the new β-CD crystals remained intact, additional testing to determine an ideal medium in which these networks would remain most stable other than ethanol could allow the use of these networks in fields such as medical treatments (as KβCD-MOF-1 was able to uptake sterols such as cholesterol and testosterone).

This project has demonstrated that unaltered β-CD can be used to make novel porous coordinate networks. Additionally cholesterol and 3 sterols have been bound to a new porous β-CD network. Although MOF crystals were not confirmed to be encapsulated within vesicles, the work in this project could lead towards research to uses of MOFs in tandem with vesicles in applications including but not limited to, transport of essential materials, removal of toxins or hazards, direct-to-cell drug delivery, specific cell to cell interactions.

References

1. L. E. Kreno, K. Leong, O. K. Farha, M. Allendorf, R.P. Van Duyne and J. T. Hupp, *Chem. Rev.* 2012. **112**, 1105–1125.
2. A. Bétard and R. A. Fischer, *Chem. Rev.* 2012. **112**, 1055–1083.
3. M. Shah, M.C. McCarthy, S, Sachdeva, A. K. Lee and H. Jeong, H. *Ind. Eng. Chem. Res.* 2012. **51**, 2179–2199.
4. Z. R. Herm, E. D. Bloch and J.R. Long, *Chem. Mater.* 2014. **26**, 323-338.
5. J. Gascon, A. Corma, F. Kapteijn and F. X. Llabrés i Xamena, *ACS Catal.* 2014. **4**, 361-378.
6. K. Sumida, D. L. Rogow, J.A. Mason, T.M. McDonald, E.D. Bloch, Z.R. Herm, T. Bae and J.R. Long, *Chem. Rev.* 2012. **112**, 724-781.
7. H. Li, M. Eddaoudi, M. O'Keeffe and O. M. Yaghi, *Nature.* 1999. **402**, 276-279.
8. P. Falcaro, R. Ricco, C. M. Doherty, K. Liang, A. J. Hill and M. J. Styles, *Chem. Soc. Rev.* 2014. **43**, 5513-5560.
9. D. Ghoshal and B. Bhattacharya, *CrystEngComm.* 2015. **17**, 8388-8413.
10. R. Ricco, L. Malfatti, M. Takahashi, A. J. Hill and P. Falcaro, *J. Mater. Chem. A*. 2013. **1**, 13033-13045.
11. P. Deria, J. E. Mondloch, O. Karagiaridi, W. Bury, J. T. Hupp and O. K. Farha, *Chem. Soc. Rev.* 2014. **43**, 5896-5912.
12. S. M. J. Rogge, A. Bavykina, J. Hajek, H. Garcia, A. I. Olivos-Suarez, A. Sepúlveda-Escribano, A. Vimont, G. Clet, P. Bazin, F. Kapteijn, M. Daturi, E. V. Ramos-Fernandez, F. X. Llabrés i Xamena, V. Van Speybroeck and J. Gascon, *Chem. Soc. Rev.* 2017. **46**, 3134-3184.
13. L. S. Murray, M. Dincă and J. R. Long, *Chem. Soc. Rev.* 2009. **38**, 1294-1314.
14. M. Ranocchiari and J. A. van Bokhoven, *Phys.Chem. Chem. Phys.* 2011. **13**, 6388-6396.
15. A. Morozan and Jaouen, F. *Energy Environ. Sci.* 2012. **5**, 9296-9290.
16. B. J. Burnett, P. M. Barron and W. Choe, *CrystEngComm.* 2012. **14**, 3839-3846.
17. C. Rösler and R. A. Fischer, *CrystEngComm.* 2015. **17**, 199-217.

18. S. Chavan, J. G. Vitillo, O. Zavorotynska, B. Civalleri, S. Jakosen, M. H. Nilsen, L. Valenzano, C. Lamberti, K. P. Lillerud and S. Bordiga, *Phys.Chem. Chem. Phys.* 2012. **14**, 1614-1626.
19. J. H. Cavka, S. Jakobsen, U. Olbye, N. Guillou, C. Lamberti, S. Bordiga and K. P. Lillerud *J. Am. Chem. Soc.* 2008. **130**, 13850-13851.
20. T. Chen, I. Popov. W. Kaveevivitchai and O. S. Milijanic. *Chem. Mater.* 2014. **26**(15), 4322-4325.
21. T. R. Cook, T. Zehng and P. J. Stang. *Chem Rev.* 2013. **113**(1), 734-777.
22. Y. Furukawa, T. Ishiwata, K. Sugikawa, K. Kokado and K. Sada. *Angew. Chem. Int. Ed.* 2012. **51**, 10566-10569.
23. A. E. Christian, M. P. Haynes, M. C. Phillips and G. H. Rothblat, *J Lipid Res.* 1997. **38**, 2264-2272.
24. P. Wallimann, T. Marti, A. Fürer and F. Diederich, *Chem. Rev.* 1997. **97**, 1567-1608.
25. R. A. Smaldone, R. S. Forgan, H. Furukawa, J. J. Gassensmith, A. M. Z. Slawin, O. M. Yaghi and J. F. Stoddart, *Angew. Chem.* 2010. **49**, 8630-8634.
26. R. S. Forgan, R. A. Smaldone, J. J. Gassensmith, H. Furukawa, D. B. Cordes, Q. Li, C. E. Wilmer, Y. Y. Botros, R. Q. Snurr, A. M. Z. Slawin and J. F. Stoddart, *J. Am. Chem. Soc.* 2012. **134**, 406-417.
27. A. Dhakshinamoorthy, M. Alvaro and H. Garcia, *Chem. Commun.* 2012. **48**, 11275–11288.
28. P. Horcajada, C. Serre, M. Vallet-Regi, M. Sebban, F. Taulelle and G. Ferey, *Angew. Chem. Int. Ed.* 2006. **45**, 5974 –5978.
29. L.A. Neves, N. Barreto, J.C. Crespo and I.M. Coelhoso, *Procedia Engineering.* 2012. **44**, 1991 – 1992.
30. J. A. Mason, M. Veenstra and J.R. Long, *Chem. Sci.* 2014. **5**, 32–51.
31. S. S. Jambhekar and P. Breen, *Drug Discovery Today.* 2016. **21**, 356-362.
32. V. J. Stella and Q. He, *Toxicologic Pathology.* 2008. **36**, 30-42.
33. K. J. Hartlieb, D. P. Ferris, J. M. Holcroft, I. Kandela, C. L. Stern, M.S. Nassar, Y. Y. Botros and J.F. Stoddart, *Mol. Pharmaceutics.* 2017. **14**, 1831−1839.
34. J. J. Gassensmith, H. Furukawa, R. A. Smaldone, R. S. Forgan, Y. Y. Botros, O. M. Yaghi and J. F. Stoddart, *J. Am. Chem. Soc.* 2011. **133**, 15312–15315.

35. B. Liu, H. Li, X. Xu, X. Li, N. Lv, V. Singh, J. F. Stoddart, P. York, X. Xu, R.Gref and J. Zhang, *International Journal of Pharmaceutic.* 2016. **514**, 212-219.
36. C. Boyer and J. A. Zasadzinski, *ACS Nano.* 2007. **1**(3), 176-182.
37. S. J. Singer. and G. L. Nicolson, *Science.* 1972. **175**(4023), 720-731.
38. G. L. Nicolson, *Biochimica et Biophysica Acta.* 2014. **1838**(6), 1451-1466.
39. M. Mihailescu, R. G. Vaswani, E. Jardon-Valadez, F. Castro-Roman, J. A. Freites, D. L. Worcester, A.R. Chamberlin, D. J. Tobias and S. H. White, *Biophysical Journal*. 2011. **100**(6), 1455-1462.
40. M. R. Krause and S. L. Regen, *Acc. Chem. Res.* 2014. **47**, 3512-3521.
41. A. Varnier, F. Kermarrec, I. Blesneac, C. Moreau, L. Liguori, J. L. Lenormand and N. Picollet-D'hahan, *J Membrane Biol.* 2010. **233**, 85-92.
42. M. Breton, M. Amirkavei and L. M. Mir, *J Membrane Biol*. 2015. **248**, 827-835.
43. L.-R. Montes, A. Alonso, F. M. Goñi and L. A. Bagatolli, *Biophysical Journal*. 2007. **93**(10), 3548–3554.
44. Z. Li, E. Mintzer and R. Bittman, *J. Org. Chem.* 2006. **71**, 1718-1721.
45. N. Cho, L. Y. Hwang, J. J. R. Solandt and C. W. Frank, *Materials*. 2013. **6**, 3294-3308.
46. P. Walde, K. Cosentino, H. Engel and P. Stano, *ChemBioChem*. 2010. **11**, 848-865.
47. G. M. Sheldrick, *Acta Crystallogr. Sect. A: Found. Adv.* 2015. **71**, 3–8. 17
48. G. M. Sheldrick, *Acta Crystallogr. Sect. C: Struct. Chem.* 2015. **71**, 3–8. 18
49. O. V. Dolomanov, L. J. Bourhis, R. J. Gildea, J. A. K. Howard and H. Puschmann, *J. Appl. Crystallogr.* 2009.**42**, 339–341.
50. J. S. Rossman, X. Jing, G. P. Leser and R. A. Lamb, *Cell*. 2010. **142**, 902-913.
51. P. Charpin, I. Nicolis, F. Villain, C. De Rango and A. W. Coleman, *Acta Cryst.* 1991. **C47**, 1829-1833.
52. I. Nicolis, A. W. Coleman, P. Charpin and C. De Rango, *Acta Cryst.* 1996. **B52**, 122-130.
53. T. Aree and N. Chaichit, *Carbohydrate Research.* 2003. ***338***, 439–446.
54. D. Balzar, *J. Res. Natl. Inst. Stand. Technol.* 1993. **98**, 321-353.
55. M. Raoov, S. Mohamad and Mhd. R. Abas, *Int. J. Mol. Sci.* 2014. **15**, 100-119.
56. D. Castagnea, G. Diveb, B. Evrarda, M. Frédérichc and G. Piela, *J Pharm Pharmaceut Sci.* 2010. **13**(2) 362 – 377.

57. G. Smith, S. Modi, I. Pillai, L. Lian, M. J. Sutcliffe, M. P. Pritchard, T. Freidberg, G. C. K. Roberts and C. R. Wolf, *Biochem J.* 1998. **331**, 783-792.

58. J. Guo, R. I. Duclos Jr. V. K. Vemuri and A. Makriyannis, *Tetrahedron Letters.* 2010. **51**, 3465–3469.

59. D. V. Waterhous, S. Barnes and D.D. Muccio, *Journal of Lipid Research.* 1985. **26**, 1068-1078.

60. S. Bekirglu, L. Kenne and C. Sandström, *J. Org. Chem.* 2003. **68**, 1671-1678.

61. F. Trotta, M. Zanetti and G. Camino, *Polymer Degradation and Stability.* 2000. **69**(3), 373-379.

62. B. Michen, C. Geers, D. Vanhecke, C. Endes, B. Rothen-Rutishauser, S. Balog and A. Petri-Fink, *Sci. Rep.* 2015. **5**, 9793.

Appendix

Crystallographic data

Tables 2 to 4 show the data obtained by Dr Shepherd, to form the structural models for Kβ-CD-MOF-1, Kβ-CD-MOF-1-Chol and Kβ-CD-MOF-2.

Table 2: Crystallographic data comparisons of Kβ-CD-MOF-1

	Calculated	Reported
Volume	6733.1(5)	6733.1(5)
Space group	P 1	P 1
Hall group	P 1	P 1
Moiety formula	C168 H280 K9 O149, 2(C H4O), 13(O)	2.25(K), C42 H70 O35, 5.5(O), 0.5(C H4 O)
Sum formula	C170 H288 K9 O164	C42.50 H72 K2.25 O41
Mr	5307.84	1326.97
Dx,g cm-3	1.309	1.309
Z	1	4
Mu (mm-1)	0.452	0.462
F000	2791	2791
F000'	2797	
h,k,lmax	19,19,37	19,19,37
Nref	55448[27724]	50757
Tmin,Tmax	0.984,0.998	0.413,0.747
Tmin'	0.977	
Data completeness	1.83/0.92	
Theta (max)	33.695	
R (reflections)	0.1136 (35439)	
wR2 (Reflections)	0.3268 (50757)	
S	1.034	
Npar	3178	

Table 3: Crystallographic data comparisons of Kβ-CD-MOF-1-Chol

	Calculated	Reported
Volume	6943.73(11)	6943.73(11)
Space group	P 21	P 1 21 1
Hall group	P 2yb	P 2yb
	C84 H139 K2.55 O74.50,	C84 H139 K2 O72.5,
Moiety formula	0.32(C27 H46 O), O0.50,O0.50, 2(O0.50),	0.55(K), 9(O), 0.32(C27 H46 O)
Sum formula	C92.64 H153.72 K2.55 O81.82	C92.64 H153.72 K2.56 O81.82
Mr	2676.55	2676.57
Dx,g cm-3	1.28	1.28
Z	2	2
Mu (mm-1)	1.651	1.651
F000	2825.3	2825
F000'	2838.43	
h,k,lmax	18,28,22	18,28,22
Nref	24538[12586]	24291
Tmin,Tmax	0.742,0.820	0.806,1.000
Tmin'	0.673	
Data completeness	1.93/0.99	
Theta (max)	66.596	
R (reflections)	0.1051 (22829)	
wR2 (Reflections)	0.2845 (24291)	
S	2.318	
Npar	1677	

Table 4: Crystallographic data comparisons of Kβ-CD-MOF-2

	Calculated	Reported
Volume	3428.78(8)	3428.78(10)
Space group	P 1	P 1
Hall group	P 1	P 1
Moiety formula	C84 H164 K3 O82, 3(C7 H5 O2), 8(H2 O)	C84 H168 K3 O84, 3(C7 H5 O2), 6(H2 O)
Sum formula	C105 H195 K3 O96	C105 H195 K3 O96
Mr	3110.92	3110.9
Dx,g cm-3	1.507	1.507
Z	1	1
Mu (mm-1)	1.953	1.953
F000	1650	1650
F000'	1657.65	
h,k,lmax	17,18,18	17,18,18
Nref	24252[12126]	21960
Tmin,Tmax	0.777,0.790	0.923,0.944
Tmin'	0.705	
Data completeness	1.81/0.91	
Theta (max)	66.594	
R (reflections)	0.0282 (21567)	
wR2 (Reflections)	0.0739 (21960)	
S	1.023	
Npar	1931	